Layered Double Perovskites

Hayden A. Evans,[1†] Lingling Mao,[2†], Ram Seshadri,[2,3,4] and Anthony K. Cheetham[2,5]

[1]Center for Neutron Research, National Institute of Standards and Technology Gaithersburg, Maryland 20899, USA. email: hayden.evans@nist.gov
[2]Materials Research Laboratory, University of California Santa Barbara, California 93106, USA.
[3]Department of Chemistry and Biochemistry, University of California Santa Barbara, California 93106, USA.
[4]Materials Department, University of California Santa Barbara, California 93106, USA.
[5]Department of Materials Science and Engineering National University of Singapore, 11907 Singapore.
[†]These authors contributed equally to this manuscript

Annu. Rev. Mater. Res. 2021. 51:1–33

https://doi.org/10.1146/((please add article doi))

Copyright © 2021 by Annual Reviews. All rights reserved

Keywords

perovskites, layered compounds, ordering, crystal structure

Abstract

Successful strategies for the design of crystalline materials that serve useful function are frequently based on the systematic tuning of chemical composition within a given structural family. Perhaps the best-known example of such a family is perovskite, ABX_3 that admit of a vast range of elements on the A, B, and X sites, associated with an similarly vast range of functionality. Layered double perovskites (LDPs) are a sub-set of this family, obtained by suitable slicing and restacking of the perovskite structure, with the additional design feature of ordered cations and/or anions. In addition to inorganic LDPs, we also discuss hybrid (organic-inorganic) LDPs here, where the A-site cation is a protonated organic amine. Several examples of inorganic LDPs are presented with a discussion of their ferroic, magnetic, and optical properties. The emerging area of hybrid LDPs is particularly rich, and is leading to exciting discoveries of new compounds with unique structures and fascinating optoelectronic properties. We provide context for what is important to consider when designing new materials, and conclude with a discussion of future opportunities in the broad LDP area.

Contents

1. INTRODUCTION

Inorganic three-dimensional (3D) perovskites, which adopt the general formula ABX_3, have had a remarkable scientific history over nearly the last 100 years,(1) spanning their use as ferroelectrics such as $BiTiO_3$,(2, 3) superconductors such as $Ba(Pb,Bi)O_3$(4) [not to exclude the perovskite-derived $YBa_2Cu_3O_x$,(5)] and materials that exhibit colossal magnetoresistance based on $LaMnO_3$.(6, 7) In recent decades, their chemistry has been extended into the realm of hybrid perovskites in which the A cation is often replaced by an amine and/or the X-site is occupied by an organic linker.(8) Important examples of the latter class include the methylammonium lead halides, $(MA)PbX_3$,(9) and dimethylammonium transition metal formates, $[(CH_3)_2NH_2]Zn^{II}(HCOO)_3$,(10) which exhibit a wide range of interesting electronic and optoelectronic properties.

One of the fascinating features of 3D perovskites is that they can often be prepared in the form of so-called double perovskites,(11) wherein, most commonly, the B-sites are occupied by two different metals in an alternating manner that resembles the rocksalt structure. These have the general formula $A_2BB'X_6$. The mineral cryolite, Na_3AlF_6 (more correctly, Na_2NaAlF_6), so important for the processing of aluminum is an example. Another is Sr_2FeMoO_6, which has attracted a great deal of interest in the condensed matter physics community on account of the unusual magnetic and electronic properties arising from the alternation of the Fe^{III} and Mo^{V} ions.(12) Again, we find analogues in the hybrid world, with recent reports of double perovskites such as $(MA)_2AgBiX_6$,(13) There are also double perovskites in which there are two different cations on the A-sites, according to $AA'B_2X_6$, such as $CaFeTi_2O_6$, as well as double-double perovskites of general formula $AA'BB'X_6$, in which there are two types of cations that are ordered on both the A-sites and the B-sites; the first detailed reported of the latter was $NaLaMgWO_6$,(14) Finally, there are both inorganic and hybrid 3D perovskites that contain two types of ordered X-anions, such as $SrTaO_2N$(15) and $[GUA]_2Mn_2(HCOO)_{1.5}(H_2POO)_{1.5}$, where GUA = guanidinium.(16) These, too, can be considered as double perovskites. **Figure 1** displays schemes of the perovskite crystal structure, and how some of the structures of interest here are derived thereof.

There is an extensive literature on 2D layered inorganic perovskites of general formula A_2BX_4, especially with X = oxygen. These are obtained by slicing the 3D perovskite and adding features that reduce the dimensionality. Classical examples include K_2NiF_4(17) and the first high temperature cuprate superconductors based on La_2CuO_4.(18) There are also

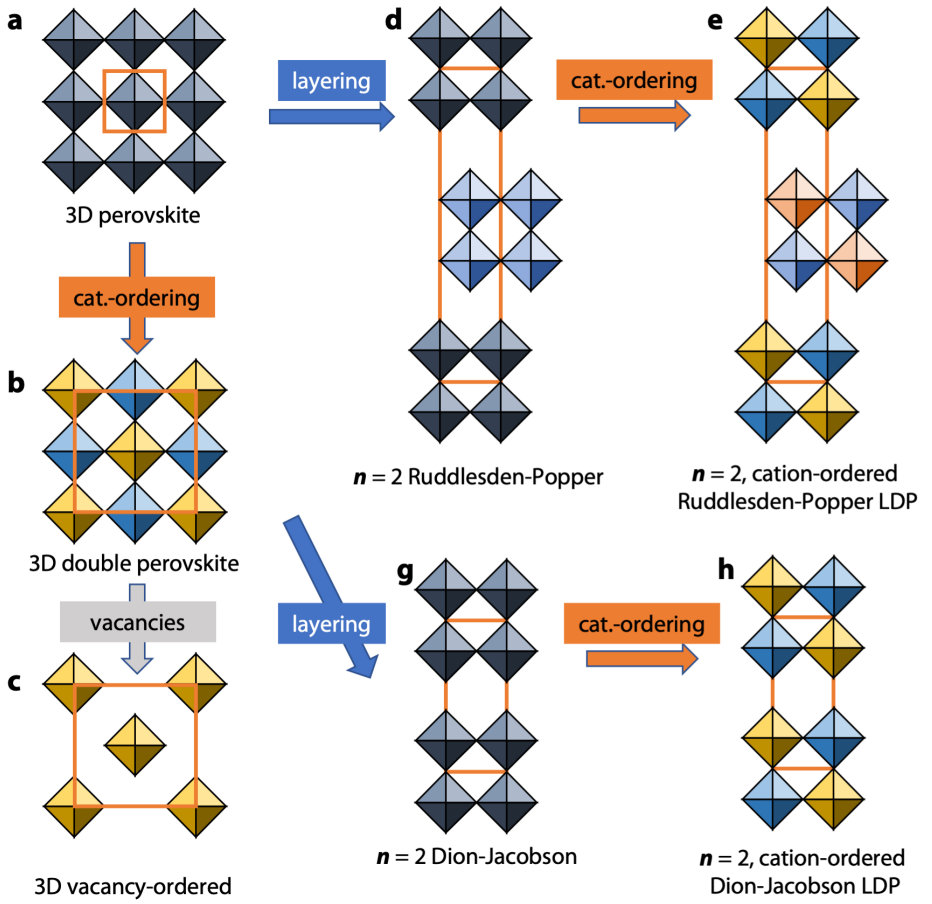

Figure 1

Schemes displaying octahedral connectivity and composition of (a) the ABX_3 3D perovskite structure, and how forking of this structure through alternating the composition of cations on the B site in an ordered manner gives rise to the $BB'X_6$ 3D double perovskite (b). If B sites are alternately skipped (left vacant) the structure of the 3D vacancy ordered perovskite A_2BX_6 emerges (c). (d) The layered Ruddlesden-Popper structure with $n = 2$. (e) The Ruddlesden-Popper LDP formed formed through cation ordering. Finally, schemes of the $n = 2$ Dion-Jacobson phase (e) without and (f) cation-ordering. The two LDPs are among the structure types emphasized here. For clarity, A species are not depicted here.

compounds with two (or more) octahedral layers of general composition $A_{n+1}B_nX_{3n+1}$, (n = 2, 3 *etc.*), such as $Sr_3Ti_2O_7$, a member of the so-called Ruddlesden-Popper (RP) series of compounds.(19). The other well-known family of layered perovskite phases is the Dion-Jacobson (DJ) series.(20, 21). Within the hybrid halide world, these have been the subject of recent attention, and were reviewed in *Annual Reviews* in 2018.(22)

The scope of this article is on compounds that combine reduced dimensionality with "doubling" as described previously. These layered double perovskites (LDPs), besides being two-dimensiional, display ordering of cations or anions on the A, B and X sites, as discussed

above for 3D systems. We restrict the discussion to compounds in which there is either full or substantial ordering on the appropriate A, B or X sites. As with the 3D systems, there are more examples of inorganic layered double perovskites than hybrid ones, although both classes are relatively new. Interesting inorganic examples include $Cs_4CuSb_2Cl_{12}$,(23) $LaSr_2Mn_2O_7$,(24, 25) and Ba_2TaO_3N.(26) We shall show that the area of hybrid layered double perovskites is particularly rich and is leading to exciting discoveries of new compounds with unique structures and fascinating properties. For example, $BA_4AgBiBr_8$ and $BA_2CsAgBiBr_7$ were recently obtained by incorporating butylammonium (BA) cations into the 3D double perovskite $Cs_2AgBiBr_6$.(27)

The first part of the review will describe all-inorganic systems, focusing on compounds that exhibit properties that are uniquely determined by the nature of their structures. In the second part, the situation with hybrid compounds is described, including a number of very recent examples that have both inorganic and organic cations on the A-sites. In closing, pointers towards areas that are ripe for further exploration are presented.

2. INORGANIC LAYERED DOUBLE PEROVSKITES

LDPs are surprisingly numerous given their strict definition. The group comprises predominantly pure oxides, but also many mixed anion phases (which understandably, are also largely oxide-derived). The range of properties in these materials is quite diverse, spanning piezoelectrics,(28) photocatalysts,(29) ion conductors,(30) thermometrics(31) and so on. There are also those which are prime candidates for post-synthetic exfoliation to create nanosheets and heterostructures, but as this is a large area of research, we will simply direct interested readers to other sources.(32, 33, 34)

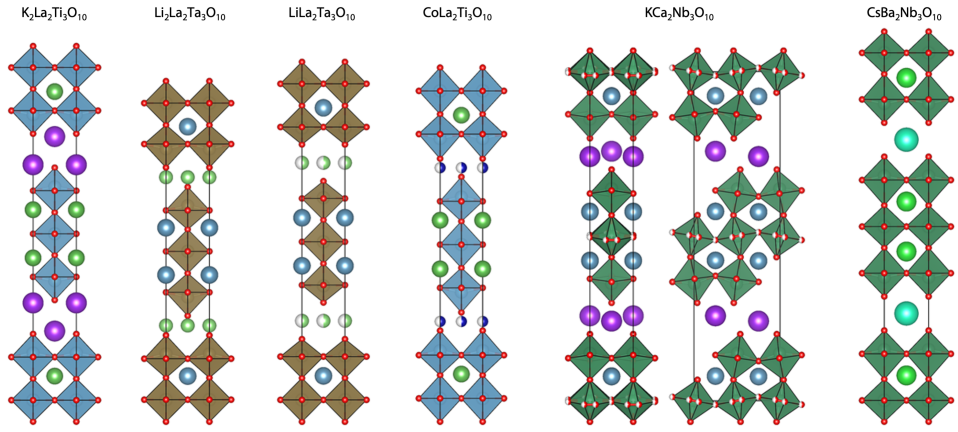

Figure 2

Depictions of various $n = 3$ compounds displaying a range of structure types, from RP to DJ, with examples of A site ordering.(35, 36, 37, 38, 39)

The sections below are broadly ordered into doubling of the A- or B-sites (AA'–B–X or A–BB'–X), those which have mixed anion sites (A–B–XX'), and then finally combinations of each. These sections are also loosely ordered by increasing n (perovskite layer thickness) where there are many examples. The compounds listed fall into three main structure

"types": Ruddlesden-Popper (RP), Dion-Jacobson (DJ),(20, 21) and (111) layered perovskites. These phases have the following general formulae: RP = $A_{(n+1)}B_nX_{(3n+1)}$, DJ = $A[A'_{n-1}]B_nX_{3n+1}$, and (111) layered perovskites = $A_nB_{n-1}X_{3n}$. We note here that RP and DJ compounds are conventionally defined by not only by the formula, but also how the perovskite slabs arrange relative to each. In the case of *A*-site ordering (**Figure 2**), one can see that the spectrum is nuanced. For this work, we will use the information of perovskite slabs that are disposed relative to each other as the main indicator of whether it is a RP or a DJ, where RP perovskite slabs are staggered, and DJ's slabs are aligned.

The goal of the inorganic section is not to provide an exhaustive list of LDPs, but instead to provide a concise survey of selected compounds that exemplify the possibilities. We discuss when one of the three possible structure types may be expected for a material, and note how certain orderings of either the *A*, *B*, or *X* sites seem to encourage one of the three structural classes. These examples should provide design principles as to what elemental compositions are available if certain structures and symmetries are sought, or conversely, what structures are attainable if certain compositional orderings are desired.

2.1. Oxide Systems

Oxide LDPs present as any of the possible structure types [RP, DJ, and (111)], with *AA'* site ordered compounds being the most common. These compounds, owing to the −2 oxidation state of oxygen, have generally high oxidation state *B*-site metals (3+ through 7+), which also accounts for the reduced variation and quantity of *B*-site ordered compounds reported.

2.1.1. AA' Oxide LDPs. Much like traditional perovskites,(40) to achieve *A*-site ordering, the charge difference of the select cations *A* and *A*' cations, and to a lesser extent the radius, needs to be sufficiently different, in order to avoid disordering over the same sites. For example, the compound $SrLa_2Sc_2O_7$ with ionic radii of Sr^{+2} and La^{+3} are 1.44 Å; and 1.36 Å;, respectively. In terms of structure type, *A*-site ordered LPDs form exclusively as either RP or DJ phases, with the final structure dictated by the ionic radii of the *A*-site cations.(41) For example, both $LiLaTiO_4$ and $KLaTiO_4$ are RP's, but how the two alkali metals order in each respective RP differs as a result of their ionic radii (CN = 8 ionic radii for Li and K are 0.92 Å; and 1.51 Å;, respectively.)(42) This size variance and final ordering can play a role for certain materials, but, in general, there is not too much difference in terms of properties between RP and DJ phases. However, one distinction is that RP phases will generally have reduced interlayer spacings relative to DJ phases, which can contribute to reduced interlayer ion mobilities,(41) reduced Brønsted acidity,(43) or impact long range magnetic ordering.

The simplest family of oxide inorganic LDPs are the RP *AA*'TiO4 compounds(*A* = H,(44) Li,(45, 46) Na,(45) K,(47, 45) Ag,(48) *A*' = rare earth,(49) which have a structure related to the prototypical RP, K_2NiF_4. As mentioned previously the *A*-site ordering differs depending on the size of the alkali metal ion size, which is a trend that is carried to higher *n* RP variants. The *AA*'TiO_4 compounds were examined in the 1990's as ion conductors ($NaLnTiO_4$),(50) as well as photocatalysts (Zr doped $KLaTiO_4$,)(51) but recent research has focused on how these compounds are also piezoelectric; the compounds being rendered polar by long-overlooked symmetry breaking octahedral rotations. (Na*A*'TiO_4(28) and LiA'TiO4 *A*' = rare earth,(52) H*A*'TiO_4,(53) K*A*'TiO_4.(54) The symmetry breaking octahedral rotations were originally rationalized using Goldschmidt tolerance factors,(1) but as

theory indicated (via a study on KA'TiO_4 the octahedral rotation instability grows when the alkali ions become larger, which is opposite to a simple tolerance factor argument.(54) It has now been proposed that the primary driving force for the octahedral rotations in KA'TiO4 is the need for optimized coordination environments for the rare-earth ions. The secondary driving force for the rotations is the interlayer lattice mismatch caused by the varying alkali metal ion sizes. Interestingly, the AA'TiO_4 compounds are the only $n = 1$ A-site ordered oxide compounds, with the only similar compounds being ordered oxyanion phases, like the recently reported Sr_2ScO_3Cl.(55) These mixed oxyanion compounds are discussed in a later section.

Similar to the AA'TiO_4 RP family are $n = 2$ compounds, like $BaEu_2Mn_2O_7$,(56) and $Rb_2LaNb_2O_7$.(57) However, instead of the RP phases, we now draw attention to the DJ AA'B_2O_7 compounds, (A = Rb, Cs; A' = rare earths, Bi; B = Nb, Ta) as they display emergent non-centrosymmetric behavior akin to the $n = 1$ AA'TiO_4 compounds.(58) Though these and similar compounds have been known for some time, ($RbLaNb_2O_7$,(57) $CsLaNb_2O_7$,(59) $RbLaTa_2O_7$,(60) $CsBiNb_2O_7$,(61, 62) alongside their (sometimes elusive) ferroelectric properties [$CsNdNb_2O_7$ and $CsBiNd_2O_7$](63) there has been a renaissance in thinking as to why RP and DJ lower dimensional compounds (not exclusively $n = 2$) are prime candidates for ferro-/piezo-electric properties.(64, 65, 66, 67) Some illuminating cases include the DJ phases of $RbNdNb_2O_7$ and $RbNdTa_2O_7$, which can be Na or Li ion substituted to create RP analogues, where $LiNdB_2O_7$ is polar,(68) as well as the DJ phase $CsBiNb_2O_7$, which is not only a Rashba-Dresselhaus ferroelectric, but one which shows promise as a "persistent spin helix" material due to its lowered symmetry.(69) Alternatively, the oxide compounds have also been shown to be used as phosphors,(60, 70) as shown for $ALa_{1-x}Ta_2O_7$:xBi^{3+},(71, 72) photocatalysts such as $RbPb_2Nb_2O_7$(29) and $Li_2CaTa_2O_7$,(73, 74) or even oxide ion conductions, as seen in $CsBi_2TiNbO_{10}$ [the Ti and Nb are disordered].(75) However, as we discuss briefly later, the symmetry breaking properties of these compounds are persistent, and even applications such as photocatalysis are impacted by induced dipoles brought about by the symmetry breaking.

The last part of the A-site ordered oxide section will focus on the $n = 3$ compounds, as higher n values can exist but are much less common. The inherent properties of the $n = 3$ compounds remain closer to the $n = 2$ variants rather than the $n = 1$, with our first examples being the non-centrosymmetric DJ phases $RbBi_2Ti_2NbO_{10}$ and $CsBi_2Ti_2TaO_{10}$.(76) These compounds are both piezoelectric, with the compound $RbBi_2Ti_2NbO_{10}$ displaying a larger corfficient of $170\,\mathrm{pm\,V^{-1}}$ [the best performing $BaTiO_3$-derived variants can display coefficients as high as $1000\,\mathrm{pm\,V^{-1}}$,(77) as well as displaying second harmonic generation with approximately 100 times the efficiency of α-SiO_2. Notable photocatalysts are also present in the $n = 3$ phases, as shown for the DJ phase, $CsBa_2Nb_3O_{10}$,(39) which according to computational results(78) is enhanced due to the inherent symmetry breaking phenomenon. This is suggested as a result of the symmetry breaking of the MO_6 octahedra from the O_h point group to centrosymmetric (D_{4h}) and non-centrosymmetric (C_{4v}) point groups, where generation of local internal fields and the promotion of electron–hole pair separation at the initial photo-oxidation step improves overall photocatalytic behavior. Similarly, $CsCa_2Ta_3O_{10}$,(79) can be nitrogen doped to be an effective visible light water oxidation catalyst,(80) and nanosheets of $HCa_2Nb_2TaO_{10}$ can be utilized for photocatalytic hydrogen-evolution.(81) As mentioned briefly in the introduction, in the case of water splitting performance, the interlayer distance within the RP and DJ compounds impacts how easily water can enter between the perovskite layers, which can either hinder or promote

kinetics.(82, 83)

Lastly, we will note some interesting magnetic properties in A-site ordered $n = 3$ oxides. The compounds $A[La_2Ti_3O_{10}]$ (A = Cu, Co, Zn,(37) Fe(84)) are one such set of compounds, and were the first layered perovskites with transition metals on the A-sites. The Fe variant in particular, has been studied for its magnetic properties, and was shown to be a spin glass below 30 K. It was found to have a frustration index (ratio between the Weiss constant and the Néel temperature) of 10, indicating a highly frustrated system. Another interesting example, albeit not for magnetic applications *per se*, is the case of diamagnetic Ru^{2+} in the compound $Na_2La_2Ti_2RuO_{10-x}$ [0< x <2],(85) in which it was found that the Na–La–Ti–O structure was capable of stabilizing the low-spin d^6 Ru^{2+}, which is rare in oxide systems.

We will conclude this section with a general thought on synthetic strategies for obtaining other A-site ordered, as well as related, compounds. A-site ordered compounds are largely prepared by conventional solid-state methods, relying on stoichiometry, difference of charge, and ionic radii to facilitate their formation. However, other methods to consider for targeting these compounds are soft chemical synthesis/intercalation methods. A few interesting examples include the transformations $K_2La_2Ti_3O_{10} \rightleftharpoons KLa_2Ti_3O_{9.5} \rightleftharpoons La_2Ti_3O_9$, where $La_2Ti_3O_9$ is an example of an interlayer A-site vacant compound,(35, 43) There is also the synthetic strategy of converting materials topotactically from lower to higher dimensional materials, such as converting $AA'TiO_4$ compounds into higher $n = 2$ variants.(86, 87)

2.1.2. BB' Oxide LDPs. There are a few examples of RP B-site ordered oxides, such as the $n = 1$ $A_2Li_{0.5}B_{0.5}O_4$ [A = La, B = Co,(88) Ni,(88) Cu,(88) Au,(89) compounds, but most form as (111) perovskites. Note the B = Cu and Au compounds above have square-planar coordination and are best described as B-site ordered Nd_2CuO_4 structures. The (111) perovskite is a type of B-site vacant perovskite structure, well known in the halides as the layered 3-2-9 phases such as $K_3Bi_2I_9$ and $Rb_3Bi_2I_9$.(90) Most B-site ordered LDP oxides present as higher n versions of (111) perovskites, predominantly the 4-3-12 phase,(91, 92) as well as what is described as $Ba_2Lu_{0.667}WO_6$ ($Ba_6Lu_2W_3O_{18}$)(93) and $Ba_2Gd_{0.33}ReO_6$ ($Ba_6GdRe_3O_{18}$) compounds,(92) which are similar to the aforementioned 4-3-12 phase, but in order to charge balance, have partial B-site vacancies. In general, we believe the reason for the higher prevalence of (111) perovskite structures relative to RP/DJ phases for the B-site ordered compounds is because the (111) structure may better stabilize the high oxidation states of the metals.

Though B-site ordering is the focus of this section, A-site compositions need mentioning as it can dictate distortions and therefore properties of the B-site ordered materials. The A-site compositions in B-site ordered oxide compounds can have just one B-site cation, as in $Ba_4BRe_2O_{12}$ (B = Mg, Ca, Co, Zn, Cd, In) and $Sr_4BRe_2O_{12}$ [B = Mg, Co, Ni, Zn].(94, 95, 96) or can be mixed/ordered, as in $Ba_3LaB^{III}(W_2O_{12})$ B = Sc, In, Lu, Yb.(97) These A-site compositions can tune magnetic properties, as in the $A_4B'B_2O_{12}$ compounds (A = Ba, Sr, La; B' = Mn, Co, Ni; B = W, Re)(96) as well as in the $A_4CoB_2O_{12}$ compounds, where different combinations of A-site cations dictate the observed ferromagnetic (FM) T_c of the system.

The B-site ordering, as one might expect, also has great significance in tuning the properties of LDP oxides. In the previously mentioned artticle on $Ba_3LaB^{III}(W_2O_{12})$ with B = Sc, In, Lu, Yb,(98) the size of the B-site metal had a direct effect on observed superlattice signatures (tripling of the unit cell), which, based on the now-known proclivity for symmetry lowering distortions in these materials, may be another example of such behavior. Similar

to the *A*-site ordering effect, magnetic interactions in these materials can also be tuned with *B*-site choice, as seen in the $Ba_2La_2NiW_2O_12$ ($Ba_2La_2BW_2O_{12}$) compounds.(96) It was found that the interactions were antiferromagnetic (AFM) for the Mn variant and ferromaghnetic (FM) for the Co and Ni variants, illustrating the competition between the FM *B*'–O–*B*–O–*B*' and AFM *B*'–O–O–*B*' superexchange interactions. Similar effects were also seen for $Ba_2La_2NiTe_2O_{12}$(99) and $Ba_2La_2NiW_2O_{12}$,(100) where the Te system is strongly antiferromagnetic and the W system is not. The reason for this discrepancy is similar, in that there are two pathways for superexchange, M^{2+} – O^{2-} – O^{2-} – M^{2+} and M^{2+} – O^{2-} – W^{6+}/Te^{6+} – O^{2-} – M^{2+}; In the W^{6+} system these two pathways cancel out, and in the Te^{6+} system they do not, which is a consequence of the differing electronic configuration of the two ions. Furthermore, at zero magnetic field, the Te system undergoes successive magnetic phase transitions at 9.8 K and 8.9 K, indicating that the ground state spin structure is a triangular structure.

Lastly, we draw attention to the compound $Ba_3La_3Mn_2W_3O_{18}$, as *B*-site ordering is dependent on the thickness of the perovskite slab and may prove to be a significant component for other designer *B*-site ordered LDPs.(101) In this work, the authors estimated the formal oxidation state of the *B*-sites by calculating bond valence in the structure, showing that the Mn ions are most likely in the +2 (+2.27) state and the two tungsten atoms are in +5(+4.89) and +6 (+6.16) states. This showed that the W^{6+} ions are located mostly on the surface of the perovskite slab, whereas the W^{5+} ions are mainly at the central octahedral layer. This type of ordering may prove to be quite significant, especially for exfoliated materials, where certain surface effects based on *B*-site ordering could be accessed.

2.2. Halide LDPs

It is interesting to note that the number of inorganic halide LDPs is quite small compared with the oxides, even though the prototypic layered perovskite, K_2NiF_4, is itself a halide. One of the few LDP fluorides that does satisfy the definition given in the introduction is $K_4Fe_3F_{12}$, which is an example of a layered (111) perovskite phase.(102) It qualifies as an LDP by virtue of its Fe^{2+}/Fe^{3+} mixed valence behavior, whereby the Fe^{2+} and Fe^{3+} cations are on different crystallographic sites. As a consequence, $K_4Fe_3F_{12}$ is ferrimagnetic below 120 K,(102) and is a Mott-Hubbard insulator.(103) The Mn analogue, $K_4Mn_3F_{12}$, is also known, albeit with a slightly different structure due to the need to accommodate the Jahn-Teller distortion of the Mn^{3+} ions.(104) It therefore exhibits both charge and orbital ordering. By contrast, the conventional RP phase, $K_3Cu_2F_7$, is also orbitally ordered,(105) but it does not technically qualify as a double perovskite because there is only one Cu^{2+} on the *B*-sites.(106) We also note that there are a few examples of layered (111) perovskite phases in which the *A*-site cations are ordered, *e.g.* $Ba_2RbFe_2F_9$.(107)

There is growing interest in LDP chlorides, bromides, and iodides at the current time due to their structural similarity to the inorganic and hybrid lead halide perovskites, such as $CsPbX_3$ and (MA)PbX_3 (X = Cl, Br, I; MA = methylammonium), which are renowned for their outstanding optoelectronic properties.(9) Although quite a number of examples of hybrid LDP chlorides have been reported, as discussed presently, practical examples of inorganic systems are few. One important exception is $Cs_4CuSb_2Cl_{12}$, which is a mixed metal (111) oriented layered perovskite that incorporates Cu^{2+} and Sb^{3+} into *B*-site layers that are three octahedra thick (*i.e.* $n = 3$).(23) $Cs_4CuSb_2Cl_{12}$ is a direct band gap semiconductor with a band gap of 1.0 eV, which is lower than that of the well-known (MA)PbI_3.

It is of significant interest in relation to the quest for non-toxic relatives of the (MA)PbX_3 family. There is also a report of $Cs_4AgBiBr_8$ and $Cs_3AgBiBr_7$, which were referred to in passing in a recent article on hybrid LDPs, but details of their properties are awaited.(27)

A closely-related example to the $Cs_4BB'_2X_{12}$ family is the series $Cs_4Mn_{1-x}Cu_xSb_2Cl_{12}$ ($x = 0$ to 1), which is again of the (111) layered perovskite type.(108) In this case, the band gap can be tuned between 1.0 eV and 3.0 eV by varying x. The $x = 0.0$ and $x = 1.0$ end members, $Cs_4MnSb_2Cl_{12}$ and $Cs_4CuSb_2Cl_{12}$, exhibit antiferromagnetic and Pauli paramagnetic behavior, respectively, due to their respective insulating and conducting properties.

In spite of the limited success in the laboratory to date, there has been recent DFT theoretical work on the $Cs_4BB'_2X_{12}$ family. For example, a recent study explored the optoelectronic potential of the $A_{n+1}B_nX_{3n+3}$ layered perovskites, focusing on the family with compositions $Cs_{3+n}B^{II}{}_nSb_2I_{9+3n}$ [B^{II} = Sn, Ge], where in this case n is the number of B(II) layers.(109) Compared to the normal two layer compound, $Cs_3Sb_2I_9$, improved band gaps, smaller effective carrier masses, larger dielectric constants, lower exciton binding energies, and higher optical absorption were predicted when inserting SnI_6 or GeI_6 octahedral layers between the Sb_2I_9 bilayers in the 2D material. It was also shown that adjusting the thickness of the inserted octahedral layers enabled tuning of the band gaps and effective carrier masses over a large range. Another recent theoretical study described a search for novel transparent conductors rather than new optoelectronic materials.(110) In a survey of 54 potential compositions (B^{2+} = Mg^{2+}/Ca^{2+}/Sr^{2+}/Zn^{2+}/Cd^{2+}/Sn^{2+}; B'^{3+} = Sb^{3+}/In^{3+}/Bi^{3+}; X = Cl^-/Br^-/I^-), seven compounds were predicted to have ideal properties for p-type transparent conductors, with $Cs_4CdSb_2Cl_{12}$ showing particular promise. There continues to be computational work in this area,(111) but there is clearly an opportunity for more progress on the experimental side.

This section on halides would not be complete without reference to an interesting variation on the theme in which the doubling of the LDP arises due to the ordering of two different halide anions.(112) $Cs_2PbI_2Cl_2$ is a classical RP layered perovskite of the K_2NiF_4 type, but with the unusual feature that the I^- and Cl^- anions are fully ordered with the iodide ion in the axial positions and the chloride ions in the equatorial sites of the BX_6 octahedra. Both DFT calculations and experimental studies indicate that other mixed anion compositions of $Cs_2PbX_2Y_2$ (X/Y = Cl, Br, I) are unstable with respect to disproportionation into alternative products. In addition to its interesting optoelectronic properties as an anisotropic wide band gap material, $Cs_2PbI_2C_{l2}$ shows promise as a high-density material for α-particle detection. The analogous tin compounds, $A_2SnI_2Cl_2$ (A = Rb, Cs) have also been reported(113) and there has been recent theoretical work on the optoelectronic properties of $Cs_2PbI_2Cl_2$ and $Cs_2SnI_2Cl_2$.(114)

Finally, we note that there have been other variations on the same theme, including the preparation of $Cs_3Bi_2I_6Cl_3$, which adopts the (111) layered perovskite structure of $Cs_3Sb_2I_9$ with Cl^- in the bridging sites and I^- in the terminal sites,(115, 116). Interestingly, the parent compound, $Cs_3Bi_2I_9$, adopts a structure containing the $Bi_2I_9^{3-}$ dimer rather than the layered $Cs_3Sb_2I_9^-$-type structure. The bromide analogue, $Cs_3Bi_2I_6Br_3$, exhibits very similar behaviour.(117)

2.3. Mixed Anion LDPs

Mixed anion systems are numerous and diverse,(118, 119) and can display interesting properties similar to their monoanion parents. However, the second anion, with its potentially

different charge, covalency, size, and coordination, offers a simple way to tune properties that are relevant to applications. As in previous sections, we will discuss select examples where the ions are ordered, and provide insight into how to make mixed anion LPDs, or how to characterize a compound to see if it has anion ordering. For example, if designing a new material, a researcher can utilize Pauling's second rule as a design guide, as discussed by Fuertes.(120) The rule states "In a stable coordination structure the electric charge of each anion tends to compensate the strength of the electrostatic valence bonds reaching to it from the cations at the centers of the polyhedral of which it forms a corner." If the known structural type (LDP in this case) and available sites/coordination numbers for the anions and cations are known, one can deduce the likelihood of ordering of specific anions. If the compound has already been made and ordering is yet to be established, we discuss methods below, particularly in the oxyfluoride section, for issues to be considered.

We will also note here that many mixed anion phases are on the edge of qualifying as LDPs. This is not for lack of ordering, but instead because some of the observed B–X bond lengths are consistently long. For example, for a lot of the oxychlorides, the metal-chloride bond lengths are often above 3 Å;, which is much longer than the expected covalent bond length of 2.4 Å; or below. Other researchers who have studied these compounds have taken contrasting views on how to view the B–X bonding; some have rationalized the compounds as LPD's with severely distorted metal-O/X octahedra,(121, 55) while other have regarded them as BO_5 square pyramids with counter X anions.(122, 123, 124) Specific to the oxyhalide field, previous research did not always take advantage of DFT calculations to support the structural characterization, but one recent work on a set of new scandium oxychlorides found that the metal halide association was essentially nonbonding, and the B cation environment is best described as square pyramidal.(125) There are, however, examples such as $CsCaNb_2O_6F$,(126) where the B-site metal-fluoride interaction is clearly bonding (bond length of 2.34 Å). In general though, a defining feature of these anion ordered LDP structure type appears to be that they are strangely effective at inducing square pyramidal geometry in metals, even for those that are not known to commonly do so (Sc and In, in particular).

2.3.1. Oxyfluoride LDPs. As oxygen and fluorine are quite similar in size, the vast majority of oxyfluoride LPDs are generally disordered.(127, 128) There are, however, a few examples which are ordered, with properties similar to their related oxide parents. The materials can be photocatalytic,(129) ionically conductive,(130) magnetically significant,(122, 131) as well as electrically conductive.(132) The observed compounds have n values of 1 or 2, including $n = 1$ compounds like $A_2(BO_3F)$ A = Ba, Sr; B = In,(133, 134, 135) Fe,(136, 137, 138) and $n = 2$ examples such as $RbLaNb_2O_6F$.(132) We were unable to find any $n > 2$ oxyfluorides that fit our criteria, but as there is a known chloride variant, $Sr_4Mn_3O_{8-y}Cl$,(123) we believe that a fluoride version is possible.

Ionic size is not the only thing that O and F have in common. They also, unfortunately, have near identical X-ray and neutron scattering cross sections, making it difficult to establish potential anion order by X-ray or neutron diffraction. This is why a local probe like NMR is commonly used to probe O/F ordering, often in conjunction with bond valence sum (BVS) calculations. As a reminder, the BVS rule states that the formal charge of a cation (anion) must be equal to the sum of the bond valences around this cation (anion). Though not always definitive and certainly not unique to the study of LPDs,(130, 132) these tactics have been employed with some success for oxyfluoride LPDs. For example, in a study of

$KSrNb_2O_6F$, Seung-Joo Kim and co-workers concluded that F ions likely fully occupy the innermost anion site within the perovskite slabs.(139) In a more recent paper,(126) the same authors compared $CsSrNb_2O_6F$ and $CsCaNb_2O_6F$ with similar methods, and again found that the F ions likely occupy the innermost position within the slabs. Ordering was also supported by the tendency of the Nb atoms to off-center towards the outside of the layers. This is not to say that all $n = 2$ oxyfluorides order similarly, but just that these examples illustrate the ways to make rational arguments, one way or another.

As a note on materials design, for the same $CsSrNb_2O_6F$ and $CsCaNb_2O_6F$ compounds,(126) the authors draw comparisons between the layered perovskites and the closely related $CsNb_2O_6F$ pyrochlore structure.(140) An important take-away is that tuning of these materials is limited, as the pyrochlore structure is quite a stable option for these oxyfluoride stoichiometries, and LPDs form only when the *A*-site cations are large enough.(141)

2.3.2. O/Cl, O/Br, and O/I LDPs. Unlike the O/F systems, the other LDP oxyhalides do not lack scattering contrast, so diffraction is an excellent way of deducing order. Furthermore, due to the differences in size and charge between O and Cl/Br/I, the likelihood of site ordering is also greatly increased. Oxychloride LDPs include $n = 1$ variants like A_2BO_3Cl where A = Ca, Sr B = Fe,(142) Mn,(143) Ni,(122) Co,(121) $A_2CuO_2Cl_2$ (A = Ca, Sr)(55, 144, 145) $n = 2$ examples such as $Sr_3Sc_2O_5C_{l2}$, and $Ba_3Sc_2O_5C_{l2}$, and an $n = 3$ compound, $Sr_8Co_6O_{15}Cl_4$.(146)

As stated in the introduction to this section, many of these Cl/Br/I compounds are close to qualifying as LDPs but are just outside our criteria, and so are only briefly mentioned. In particular, the $n = 1$ $Sr_2CuO_2Cl_2$ compound is an antiferromagnetic material,(147) but can be easily made into a high temperature superconductor with slight Na doping. There are also examples of the Br compounds Sr_2FeO_3Br(138) and $Sr_2CoO_2Br_2$(148)) and the I compound such as ($Sr_2CuO_2I_2$(149) of similar structure, as well as $n = 2$ and $n = 3$ compounds, but as the halides do not actively participate in any electronic coupling (due to their axial positions), many properties of the Br/I compounds are quite similar to their Cl counterparts.

2.3.3. Oxysulfide and related LDPs. Oxysulfides LDPs (or even just LP sulfides) are quite rare. This is because the *B*-sites metals (commonly mid-transition elements) when paired with sulfur often have a proclivity to stabilize with lower oxidation states and favor tetrahedral rather than octahedral coordination. However, there are a few examples, with the expected caveat of long *B*-site metal – S bonds. These include $Tb_2Ti_2O_5S_2$,(150) $Sm_2Ti_2S_2O_{4.9}$,(151) $Ln_2Ti_2S_2O_5$ (Ln = Nd, Pr, Sm),(152) as well as $KY_2Ti_2O_5S_2$.(153) One material of note, $Y_2Ti_2O_5S_2$, has been shown to be an effective photocatalyst capable of stoichiometric water splitting following spatially separated loadings of IrO_2 and Cr_2O_3/Rh as the oxygen and hydrogen evolving complexes, respectively.(154)

2.3.4. O/N and related LDPs. Metal oxynitrides, not just specifically LDPs, are an emerging class of materials with captivating photocatalytic and electronic properties.(155, 156, 157, 158) Their success as photocatalysts, for example, comes in part from having red-shifted absorption edges relative to their oxide counterparts, which increases visible light absorption and leads to improved photocatalytic efficiency. In terms of oxynitride LDPs, there are a few examples of mention, including the $n = 1$ RP tantalate compounds, $Ba_2TaO_3N_10$.(26)

and Sr_2TaO_3N,(159) and related niobates, such as Sr_2NbO_3N.(160) In the manuscript from Rosseinsky and coworkers on Ba_2TaO_3N,(26) the authors demonstrated that if Ba_2TaO_3N was made conventionally, the O and N atoms were disordered, but if the N source is made with a mineralizer present, that the anions will order. Specifically, the equatorial anion sites within the $n = 1$ perovskite layer are predominantly populated by nitrogen, and the apical sites are occupied by oxygen. This ordering is also achievable for Sr_2TaO_3N.(161, 162, 163) These oxynitride phases exhibit high bulk dieletric constants, as do other related compounds with the general formula ABO_2N (A = Ba, Sr, Ca; B = Ta, Nb), as shown by Tai and coworkers.(164) Other interesting phases include a recent example like the compound $Eu^{II}Eu^{III}{}_2Ta_2N_4O_3$, which was made through high temperature and pressure autoclave synthesis.(165) This material has a small (assumed direct) band gap of 0.6 eV, but has yet to be studied in great detail in terms of its potential optoelectronic or other properties. As a final underexplored example, there is the known compound Nd_2AlO_3N.(166) No properties were reported for the material, but it is known to crystallize in the polar space group, $I4/mm$ (109), and may therefore warrant further exploration.

2.3.5. O/OH LDPs. Much like the oxyhalides and oxysulfides, LDP oxyhydroxides can display long B-site metal–OH bonds. Numerous LDP oxyhydroxides appear to have been inspired by the topotactic conversion of the iron based layered oxide, $Sr_3NdFe_3O_{8.5+\delta}$, into the hydrated oxyhydroxide, $Sr_3NdFe_3O_{7.5}(OH)_2{\cdot}H_2O$, and studied for their magnetic properties.(167, 168, 169) In the case of $Sr_3NdFe_3O_{7.5}(OH)_2{\cdot}H_2O$, the hydroxide compound forms upon exposing the oxide parent, $Sr_3NdFe_3O_{9-\delta}$, to humid air over multiple days, and the hydroxide ions order at the apical sites of the perovskite layer. This procedure is essentially the same for all other hydroxides which form topotactically from oxide parents. In the manuscript from Maignan and coworkers,(170) the authors demonstrated that the perovskite layer thickness (and concomitant strength of magnetic interactions) in the oxide/oxyhydroxides Sr-Co-Ti-O system [the example being $Sr_3(Co{+}1.7Ti_{0.3}O_5(OH)_2){\cdot}2(H_2O)$] were controlled by the Ti/Co ratio. A later manuscript from some of the same authors showed just how impactful the topotactic conversion could be on magnetic properties. For example, the oxyhydroxide, $Sr_{3-\delta}Co_{1.9}Nb_{0.1}O_{4.86-\delta}(OH)_{3.04}{\cdot}0.4H_2O$, was found to be a weak ferromagnet with a $T_c \approx 200$ K, even though its parent oxide was a spin glass material with a $T_g \approx 50$ K.(171)

2.3.6. O/H LDPs. The oxyhydrides are an incredibly interesting class of LDPs, with both magnetic and ion conducting functionalities.(172) We will start with the notable example of $LaSrCoO_3H_{0.7}$ reported by Hayward *et al.*, which was prepared by the reaction between $LaSrCoO_4$ with CaH_2.(173) This compound is quite remarkable in that it has magnetic long-range order above room temperature, a result of the capacity of the hydride anions to strongly couple transition metal cations electronically. The hydrides present a clear distinction in this respect to other $n = 1$ ordered anion phases (except the nitrides and a few fluorides), as the hydride ion orders equatorially in the B-site perovskite layer, whereas the majority of other anions prefer to order at apical sites (and far away from the metal, as we have seen). This ultimately eliminates most anions from participating in magnetic coupling between the perovskite layers, making the hydrides an attractive class of materials for tuning electromagnetic properties. There are, however, instances where, if the hydride ions are low enough in concentration (not necessarily LPDs), then the hydride site preference depends on the n value.(174)

Although examples of LDP oxyhydrides were first synthesized three decades ago,(175) some have recently also shown promise as high performance ionic conductors.(176, 30) Interestingly, for the LDP oxyhydride, Ln_2LiHO_3, hydride ion conduction pathways were found to unlike the related oxide conducting counterparts, such as La_2NiO_4.(177) The reason for the difference is thought to be that the increased covalent character of the La-O layer of the oxyhydride creates barrier channels of electron density in the structure, ultimately making in-plane migration the more favorable energy pathway for hydride migration. For oxide anions in La_2NiO_4 and other similar oxides, the ions move via an interlayer path. As the interlayer path should be more efficient, materials like $Ba_2MgH_2O_2$ and $Sr_2MgH_2O_2$ have been proposed as better hydride ion conductors as there is decreased covalent bonding between Mg and O.

2.3.7. Other Mixed Anion LDPs. There are also examples of LDP compounds which fall just outside of the descriptions we have given above. Some of these include combinations of halides and polyatomic anions, like $Cs_2PbI_2(SCN)_2$.(178) This compound, as well as its hybrid cousins,(179, 180) have been studied as possible alternatives (due to their stability) to the 3D connected hybrid halide perovskites. There are also examples of LDP nitrofluorides, like the first reported $Ce_2MnN_3F_{2-\delta}$.(181) The preparation of this compounds is quite interesting, as it was made by low-temperature fluorination of the ternary nitride, Ce_2MnN_3. It was shown by a combination of neutron diffraction and magnetic susceptibility studies to have mixed valence Mn and fluoride ion interstitials within a K_2NiF_4-type structure.

3. HYBRID LAYERED DOUBLE PEROVSKITES

Hybrid LDPs are LDPs which contain organic species on at least one of the A, B, or X sites. As B-sites are populated almost exclusively with metals cations, the A and X sites provide the most variation for organic substitution. Hybrid LDPs can be further characterized into four main categories: AA'-Type I, AA'-Type II, BB', and XX', as illustrated in **Figure 3**, which displays the relevant schemes. In **Figure 4**, the different amine cations that are frequently found to assist in teh formation of LDPs are depicted. As we have done for the inorganic sections, we have selected representative cases from each category, and assess areas of possible expansion for new materials.

3.1. AA' Hybrid LDP Halides

3.1.1. AA'-Type I hybrid LDPs. The AA'-type ordering is unique to hybrid LDPs and is characterized by having both A and A' cations ordered within the same interlayer space ($n = 1$ LDPs only). As a general note, if the compounds have the same perovskite layer orientation/composition, the materials will usually have similar properties regardless of the A-site cations of choice. However, as many organic cations have variable size and functionality, changing between organic cations can inadvertently template new perovskite layer orientations, and therefore change properties. This templating effect is a defining feature of the AA'-type I compounds and is what gives rise to the cation ordered (100)-, (110)- and (210)-oriented structures seen in **Figure 5**. With more perovskite layer orientations (in addition to the RP and DJ phases seen in the inorganic section), hybrid LDPs display a great degree of structural and synthetic variability. For instance, Nazarenko *et al.* reported combining guanidinium (GA) and smaller cations [Cs or methylammonium (MA)] to obtain

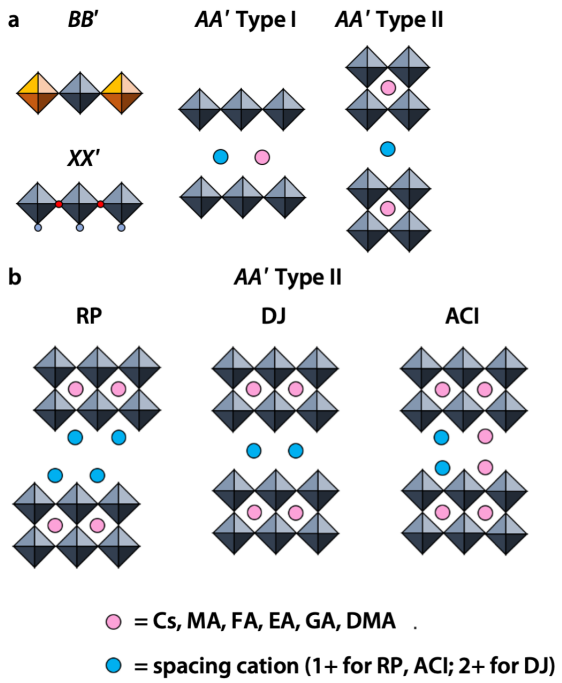

Figure 3

(a) Schematic illustration of different types of hybrid layered double perovskites: *BB'* involving ordering on the metal *B* site, *XX'* involving ordering on the linkers, and two kinds of *AA'*-type I with cations ordering between the layers and *AA*'-type II with cations ordering within and outside the cages. (b) Schematic illustration of *AA*'-type II structures, RP, DJ, and ACI.

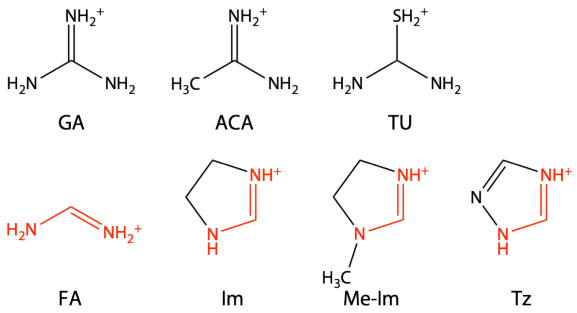

Figure 4

Some of the amine cations that are commonly employed in the stabilization of layered hybrid halide perovskite compounds, including hybrid LDPs.(182, 183, 184, 185, 186, 187, 188, 189)

(100)-oriented structures like (GA)$CsSnBr_4$ and (GA)(MA)PbI_4,(182, 183) whilst others have reported that by using a larger *A*' cation such as imidazolium (Im), methylimidazolium (Me-Im) or triazolium (Tz), (110)-oriented structures like (GA)(Im)$PbBr_4$, (GA)(Im)$PbBr_4$ and $(GA)_{1.5}$(Me-Im)$_{0.5}SnI_4$ can be made.(184, 185) There are also examples with mixed

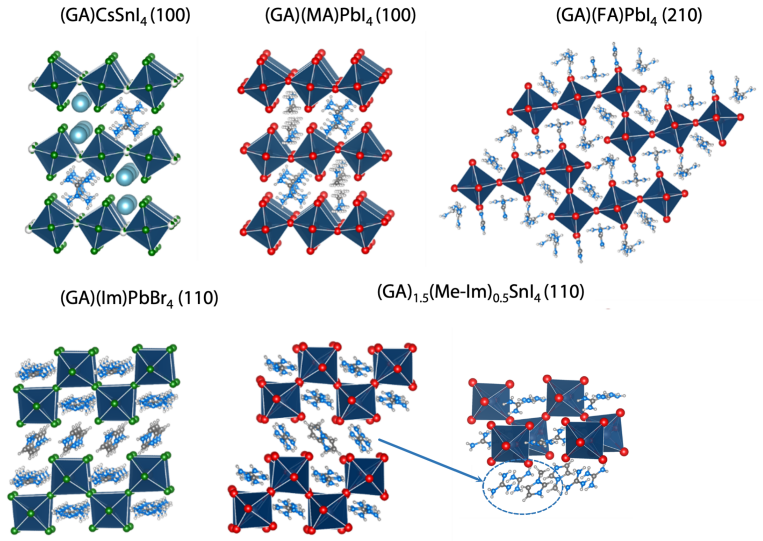

Figure 5

Example structures with different types of either (100),(182, 183) (210),(188, 189) or (110)(184, 185) layer orientations.

A site cations, such as $(GA)_{1.5}(Me\text{-}Im)_{0.5}SnI_4$, where the stoichiometry is nontypical as GA cations share the same cavities with Me-Im cations. To our knowledge, there are no inorganic LDP examples similar to $(GA)_{1.5}(Me\text{-}Im)_{0.5}SnI_4$. There are also instances of (110)-oriented structures, including $(HEA)(FA)PbBr_4$ (HEA = hydroxyethylammonium), reported by Salah *et al.*(186) Guo *et al.* recently reported a "3×3" type (110)-oriented compound $[ImH][TzH]PbBr_4$ ($[ImH^+]$ = imidazolium, $[TzH^+]$ = 1,2,4-triazolium).(187) The (210)-oriented type is the least common of the possible perovskite orientations and was first demonstrated by Nazarenko *et al.*(188) and Daub and Hillebrecht in 2018.(189) Both groups reported the structure of $(GA)(FA)PbI_4$, but Daub and Hillebrecht also reported $(Tu)(FA)PbI_4$ [Tu = [protonated thiourea], which formed with the same (210)-oriented structure.(189) This is not too surprising given that GA and Tu are similar in shape, size, and functionality, and would be expected to have similar templating effects (see the Sidebar on amines).

From these observations, we can generalize a structural trend: GA/Tu/ACA [acetamidinium] plus a small cation like Cs or MA will create a (100)-oriented compound; GA/Tu/ACA plus a larger cation (with similar functional group identity highlighted in red the Sidebar on amines) will create either (210)- or (110)-oriented type LDPs. This suggests there are plenty of opportunities to create new structures using the less explored Tu and ACA cations, but also note that stoichiometry plays a vital role in designing these hybrid compounds. For example, when the ratio of *AA*' cations change from 2:1, 1:1 to 1:2, the structures can be distinct with potentially more than one cation occupying multiple sites within the structure.

3.1.2. Type-II AA'. The type II *AA*' double perovs.kite is defined by *A* cations occupying the perovskite cages, and the *A*' cations (as well as *A* cations in some cases) ordering

between the perovskite layers. phase is similar to *AA*'-type I, where both *A*' and *A* cations are found in interlayer sites, but also with *A* cations in the perovskite cages. In most cases of RP, DJ, and ACI structures, the *A* cations and *A*' spacing cations are different species, so that the way they formed qualifies as naturally *AA*'-Type II, as shown in **Figure 3**, except for $(EA)_4Pb_3Cl_{10}$, $(EA)_4Pb_3Br_{10}$ and $(IPA)_3Sn_2I_7$ (EA = ethylammonium, IPA = isopropylammonium). There are extensive examples of layered perovskite RP, DJ and ACI phases, which has been covered previously in other reviews.(190, 191, 192)

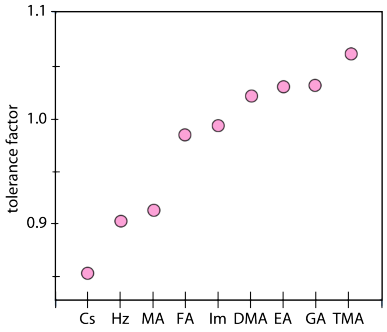

Figure 6

The perovskite tolerance factor of the smaller *A* cations employed in the preparation of hybrid LDPs. Adapted from reference (193).

In regards to *A* site cation choice, a particularly recent and interesting discovery in 2D halide perovskites is that *A* cations (within the perovskite cages) are not limited to methylammonium (MA), formamidinium (FA) or Cs, unlike for 3D perovskites. Fu *et al.* first reported a series of $n = 2$ compounds, $(HA)_2(A)Pb_2I_7$, where HA is n-hexylammonium and *A* = MA, FA, DMA, EA, GA, and AA (DMA = dimethylammonium, GA = guanidinium and Aa = acetamidinium).(194, 195) Among these compounds, the examples where *A* = DMA, EA, GA and Aa all have tolerance factor ratios of above 1 (**Figure 6**),(194) which contrasts with the usual Goldschmidt tolerance factor guideline of values between 0.8 to 1.0. The more lenient tolerance factor requirement here is attributed to the flexibility of the 2D framework, as strain can be accommodated more easily by the 2D RP structures. There are also $n = 3$ structures that have been made, such as $(BA)_2(EA)_2Pb_3I_{10}$,(196, 197) where the EA-based structure displays blue-shifted absorption and photoluminescence due to the larger distortion in the inorganic framework. Li *et al.* subsequently expanded upon this work, and reported the $(BA)_2(A)Pb_2I_7$ series (*A* = MA, FA, DMA and GA), showing this rule also applies when changing the spacing cation to BA.(198)

3.2. BB' Hybrid LDP Halides

A defining feature for LDPs, and hybrid LDPs especially, is that for certain *B* or *X* site compositions where a 3D perovskite phase is unstable, a 2D analogue may still form. For example, the iodide-based double perovskite Cs_2AgBiI_6 has not yet been synthesized, partially due to having an unfavorable tolerance factor value and also because it is competing against the favorable formation of $Cs_3Bi_2I_9$. However, several iodide hybrid LDPs have been made. These phases include $[AE2T]_2AgBiI_8$, $(CHDA)_2AgBiI_8$, $(AMP)_4AgBiI_8$, $(IPA)_4AgBiI_8$ (AE2T = 5,5-diylbis(amino-ethyl)-[2,20-

bithiophene]), CHDA = 1,4-cyclohexanediammonium, AMP = 4-aminomethylpiperidinium, IPA = 3-iodopropylammmonium) and more (see **Table 1**). The first case of an iodide-based hybrid LDP was $(AE2T)_2AgBiI_8$, reported by Jana *et al.*, in which the di-cation AE2T was employed.(199) Bi et al. subsequently reported a series of I-based hybrid LDPs, with the *B*-site being either Cu or Ag, and B' being Bi, and the A-site spanning a series of mono- and di-cations.(200, 201) This increased stability window, especially in the case of the iodides, is related to the aforementioned capacity to bypass the tolerance factor limitations of the *A*-site. The recent development of hybrid LDP halides was catalyzed by a report from Connor *et al.,* who demonstrated dimensionality-reduction of the 3D double perovskite $Cs_2AgBiBr_6$ by incorporating butylammonium (BA) into the synthesis; this resulted in the formation of $(BA)_4AgBiBr_8$ (single-layered, $n = 1$) and $(BA)_2CsAgBiBr_7$ (double-layered, $n = 2$).(27)

In addition to the more predictable phases derived from 3D double perovskites, such as $(BA)_4AgBiBr_8$ (parent: $Cs_2AgBiBr_6$), and $(PA)_4AgInCl_8$ (PA = propylammonium) (parent: $Cs_2AgInCl_6$), unexpected phases like $(PA)_4AgInBr_8$ (parent compound $Cs_2AgInBr_6$ has not been reported) have been demonstrated. More new phases are expected to be made, either from adding different organic spacer cations to existing 3D systems, such as the compounds listed in Table 1, or by using different octahedrally coordinated *B* (1+) and *B*' (3+) cations, as shown in **Figure 5**. Typical 1+ metal cations that can adopt octahedral geometry include the alkali metals Na, K (Li is usually too small and Rb, Cs too large) or the coinage metals Cu, Ag and Au. Metals that can be 3+ with octahedral coordination include Sc, Y, Ti, V, Cr, Mo, Fe, Ru, Co, Au, lanthanides, actinides, and group III elements.

Though the organic layer can impact properties by templating the perovskite layer, the optical and electronic properties of the *BB*' type hybrid LDPs are more dependent on the metal and halide composition. In a system where only the thickness of the layer varies, such as $(BA)_2Cs_n(AgBi)_nBr_{3n+1}$, the band gap (absorption edge) of the $n = 1$, 2 compounds, and the 3D parent $Cs_2AgBiBr_6$, are ≈2.6 eV, ≈2.4 eV and ≈2.2 eV, respectively.(27) Compared to a Pb-based system like $(BA)_2(MA)_{n-1}Pb_nBr_{3n+1}$, the jump between $n = 1$ and 3D has a much more significant effect on the optical properties. The bandgap decreases from ≈3.0 eV ($n = 1$) to ≈2.25 eV (3D $(MA)PbBr_3$).(211) As such, there has been a drive to increase the layer thickness of both hybrid LDPs as much as possible. This, however, is difficult, and to-date there have not been any reports of new *B*-site ordered hybrid LDPs with $n > 2$.

For *B*-site ordered materials, the role of the organic cation is often marginal. In a previous report from some of the authors of this work,(202) organic *A* cations propylammonium (PA), butylammonium (BA), octylammonium (OCA) and butyldiammonium (BDA) based $A_nAgBiBr_8$ ($n = 1$ or 2) materials have similar bandgaps in the range of 2.41 eV to 2.45 eV. Woodward and coworkers also reported four hybrids with BA as spacing cation, where they used solid-state synthesis to make $(BA)_4CuInCl_8$, $(BA)_4AgInCl_8$, $(BA)_4AgSbCl_8$, and $(BA)_4AgSbBr_8$.(203) Likewise, Bi et al. reported a series of A_nCuBiI_8 ($n = 1$ or 2) materials with different organic cations, where the bandgap of the materials span a narrow range between 1.55 eV to 1.65 eV.(201) An interesting discovery from both reports though is that materials with larger interlayer distances generally have slightly larger bandgaps. Another characteristic observed by Bi *et al.* is that the bandgap increases with smaller Cu–I–Bi angles, making it similar to Pb- or Sn-based 2D systems, where larger *B*–*X*–*B*' angles correspond to smaller bandgaps.(ref) However, of the two structures reported, the Cu atom is split (disordered) on average, making the Cu–I–Bi angles from two of the structures difficult

Table 1 Summary of optical and electronic properties of reported 2D hybrid double perovskite to-date.

Compound	E_g (eV)	Electronic structure
Cl-based		
$(PA)_4AgInCl_8$(202)	3.96	indirect
$(BA)_4AgInCl_8$(203)	4.27	N/A
$(BA)_4CuInCl_8$(203)	3.47	N/A
$(BA)_4AgSbCl_8$(203)	3.22	N/A
Br-based		
$(BA)_4AgBiBr_8$(27)	2.60	direct
$(PA)_4AgBiBr_8$(202)	2.41	inconclusive
$(OCA)_4AgBiBr_8$(202)	2.45	N/A
$(BDA)_2AgBiBr_8$(202)	2.43	inconclusive
$(Cl\text{-}PA)_4AgBiBr_8$(204)	2.57	indirect
$(PA)_4AgInBr_8$(202)	3.15	indirect
$(BA)_4AgSbBr_8$(203)	2.80	N/A
$(3\text{-}BPA)_4Ag$*B*Br_8, *B* = In, Tl(205)	≈3.25, 2.25	indirect
$(BA)_2CsAgTlBr_7$(205)	≈2.1	direct
$(PEA)_2CsAgTlBr_7$(205)	≈1.9	direct
$(BA)_2CsAgBiBr_7$(27, 206)	2.38	indirect
$(PA)_2CsAgBiBr_7$(202, 207)	2.32	inconclusive
Br-based		
$[NH_3(CH_2)8NH3]_2$ $[(AuI_2)(AuI_5)(I_3)_2]$(208)	1.14	N/A
$(AE2T)_2AgBiI_8$(199)	2.0	direct
$(CHDA)_2$*B*BiI_8, *B* = Ag, Cu(200)	1.93, 1.68	indrect
$(CAA)_nCuBiI_8$ (n = 2 or 4)(201)	1.5-1.6	direct
$(IPA)_4AgBiI_8$(209)	1.87	indirect
$(AMP)_4AgBiI_8$(210)	2.0	direct
$(APP)_4AgBiI_8$(210)	2.05	direct

to quantify on a local scale. Nevertheless, in this instance, the organic cations have some impact on the overall structure and properties of the hybrid LDP systems. The direct and indirect effects need to be evaluated on a case-by-case basis, but between templating or changing interlayer space, their role can sometimes be benign, or sometimes impactful.

That said, a wide range of property tunability is possible for *B*-site ordered hybrid LDPs, with bandgaps spanning a remarkable 2.3 eV (≈1.7 eV to ≈4 eV) depending on the choice of halide. The bandgaps are smallest and largest for chloride and iodide materials, respectively. However, finer tuning of the optical properties is possible by changing the *B*-site metal composition, as demonstrated with $(CHDA)_2CuBiI_8$ (≈1.68 eV) and $(CHDA)_2AgBiI_8$ (≈1.93 eV).(201) Thus, by changing the *B*-site cation (1+) from Cu to Ag, one can enlarge the bandgap. This behavior is also demonstrated in the cases of $(BA)_4CuInCl_8$ and $(BA)_4AgInCl_8$, where the band gap increases from ≈3.47 eV (Cu) to ≈4.27 eV (Ag).(27) In the BA-based bromide systems, the corresponding *B*' cation varies from In, Sb to Bi; these compounds show a bandgap trend of In > Sb > Bi, where $(BA)_4AgInBr_8$, $(BA)_4AgSbBr_8$ and $(BA)_4AgBiBr_8$ have bandgaps of ≈3.32 eV, ≈2.80 eV and ≈2.65 eV, respectively.(203, 27)

Particularly interesting cases of hybrid LDPs include some of the following. In

2003, Guloy and co-workers reported a special type of hybrid layered double perovskite, with mixed valent Au^{I} and Au^{III}: $[NH_3(CH_2)_8NH_3]_2[(Au^{I}_2)(Au^{III}_4)(I_3)_2]$ and $[NH_3(CH_2)_7NH_3]_2[(AuAu^{III}_2)(Au^{III}_4)(I_3)_2]$.(208) In these compounds, $[Au^{I}6]$ octahedra are compressed tetragonally whereas the terminal iodides in $[Au^{III}6]$ are composed of partial polyiodides I_3^-. The optical band gaps for these compounds are ≈1.14 eV and ≈0.95 eV, respectively, which is lower than $Cs_2Au_2I_6$ (≈1.31 eV) or presumably $(MA)_2(Au_2I_6)$,(212) this can potentially be explained by the incorporation of I_3^-. There is also the recently reported I-based hybrid, $(IPA)_4AgBiI_8$, where the spacing cation IPA was originally 3-bromopropylammmonium, which reacted *in situ* with hydroiodic acid to become 3-iodipropylammonium.

There have been several computational studies of hybrid LDPs using Density Functional Theory (DFT). The calculated electronic structure of the 3D double perovskite $Cs_2AgBiBr_6$ has an indirect bandgap, where the conduction band minimums (CBM) consist of Ag s, Bi p and Br p orbitals, and the valence band maximums (VBM) consist of Ag d, Bi s and Br p orbitals.(213, 206) When Connor *et al.* reported the hybrid LDP derivatives of $Cs_2AgBiBr_6$ [$n = 1$ compound $(BA)_4AgBiBr_8$, and $n = 2$ compound, $(BA)_2AgBiBr_7$](27) calculations showed similar frontier orbital composition to the 3D parent compound, but where, interestingly, the $n = 1$ compound had a direct bandgap. The authors attributed this indirect-to-direct change explicitly to the dimensionality reduction. Conversely, Tran *et al.* reported a counter example of a direct-to-indirect change of a bandgap by replacing In with Sb in $Cs_2AgSb_xIn_{1-x}Cl_6$ solid solutions.(214) Their calculations showed that $Cs_2AgInCl_6$ had a direct bandgap, and that by increasing the amount of Sb, the CBM became defined by the Sb 5p orbital (transition observed at $x = 0.4$), and the transition became indirect. It has also been shown that for the PA (propylammonium) end member compound of the same *B*-site composition, $[(PA)_4AgInCl_8]$, calculations indicate the bandgap to be indirect.(202) Additionally, it was reported that because of the relatively flat bands, the bandgap of the related compound $(BDA)_2AgBiBr_8$ was difficult to discern as either direct or indirect.(202)

Similarly, when Jana *et al.* reported the first iodide based hybrid layered double perovskite, $(AE2T)_2AgBiI_8$, the calculated band gap was reported to be indirect without spin orbit coupling (SOC), but direct with SOC.(199) More recently, Karunadasa and coworkers reported the $n = 2$ structure $(PEA)_2CsAgTlBr_7$, (PEA = phenethylammonium), had a direct bandgap, where the VBM is composed of Ag d and Br p orbitals, and the CBM is composed mainly of Tl s and Br p orbitals, similar to the 3D double perovskite $Cs_2AgTlBr_6$.(205) The bandgap of the $n = 1$ compound, however, was found to be indirect, originating from Ag-to-Tl metal charge transfer. A more detailed list of the reported layered double perovskites and the nature of their electronic structures can be found in Table 2.

In general, when compared to the Pb- or Sn-based layered perovskites, the hybrid LDPs generally have flatter bands. The situation is therefore not as clear as in the Pb- or Sn-based systems, where the materials have direct bandgaps. From the results on hybrid LDPs, we can see that the nature of the bandgap is highly dependent on the metal composition. Layer thickness and local structural distortion may also play a part in determining the direct/indirect transition. Careful theoretical work is needed before generalizing the trend base on the parent 3D material or simply on the dimensionality reduction.

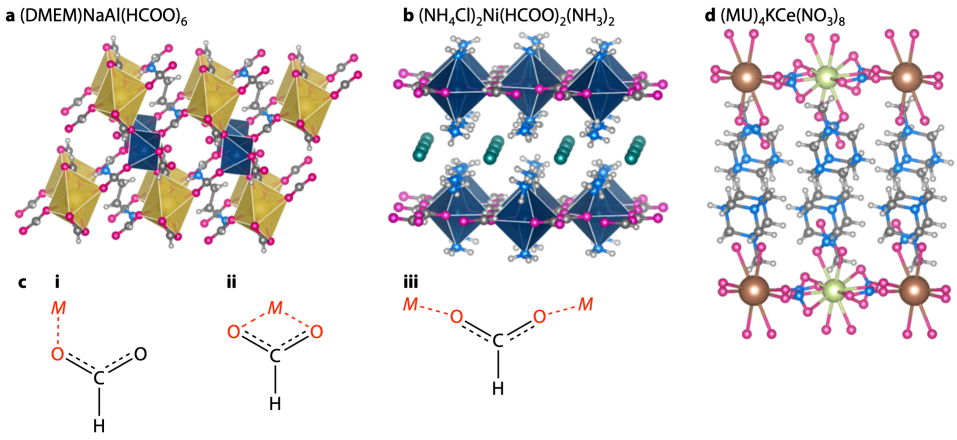

Figure 7

Crystal structure of (a) (DMEN)NaAl(HCOO)$_6$(215) and (b) [NH$_4$Cl]$_2$[Ni(HCOO)$_2$(NH$_3$)$_2$].(216) (c) Depiction of the different modes of formate coordination modes with metals. (d) Crystal structure of (MU)$_4$KCe(NO$_3$)$_8$.(217)

3.3. Hybrid LDPs with Polyatomic Anion Linkers

Only a few examples of hybrid LDPs with organic or polyatomic linkers on the X-sites are known. In principle, it is possible to form these layered structures with linkers such as formate, nitrate, azide, imidazolate, cyanide etc, as they have been well documented to make perovskite type structures with suitable single metal compositions.(218, 8) Contrary to the many halide examples discussed earlier, however, the coordination between the metal and X-site linker in hybrid LDPs can display multiple types of coordination modes, often creating more complex structures. A layered double perovskite formate with Na^+ and Al^{3+} using the cation DMEN (DMEN = N,N'-dimethylethylenediammonium) (**Figure 7a**) has been reported.(215) The coordination modes between the formate linkers and the metals in (DMEN)NaAl(HCOO)$_6$ are also listed, illustrating the multiple (i, ii and iii) types present in the structure. This contrasts with the bonding seen for formate perovskites, or the analogous hypophosphite perovskites and ReO$_3$-type structures.(219, 220, 221) Understandably, the possibility of several bonding modes makes designing a layered structure difficult, as the formation of a more extended and complex structure may result depending on the metal and A-site cation of choice. However, multiple X-site anions can be included to diminish this effect. For example, in the case of the X-site ordered hybrid LDP, [NH$_4$Cl]$_2$[Ni(HCOO)$_2$(NH$_3$)$_2$] (**Figure 7b**),(216) the formate links the Ni atoms together in the equatorial positions and ammonia caps Ni at the axial positions. In this example, only the easily-understood bonding mode iii is present (**Figure 7c**).

Another recent example used nitrate as the bridging linker (with doubling on the B-site) to yield a series of new compounds.(217) Shi et al. found that by using chiral R/S-3-fluoroquinuclidinium, R/S-3-chloroquinuclidinium, and R/S-4-fluoro-1-azabicyclo[3.2.1]-octanium cations, noncentrosymmetric structures could be made. They investigated multiple B^{I} and B'^{III} combinations, such as K^+ with Ce^{3+} (**Figure 7d**), Rb^+ with Tb^{3+}, Dy^{3+}, Eu^{3+} and Sm^{3+}, and Cs^+ with Sm^{3+}. Interestingly, NH_4^+ can also act as a 1^+ cation on the B-site, and formed an hybrid LDP structure with Ce^{3+}. The discovery of noncentrosym-

metric, SHG active materials combined with the emissive nature of the rare earth metals opens up a new pathway to engineer multifunctional hybrid materials.

4. Conclusion

In this review of layered double perovskites, we have laid out a case for the hitherto unrecognized richness of structure in this large family of crystalline compounds, accompanied by an equal wealth of properties, whose tuning is accomplished through the many different compositional knobs that can be turned. The accompanying Summary Points capture the essence of what has been covered, and the Future Directions outline promising avenues of research in the area of LDPs.

SUMMARY POINTS

1. The chemical diversity of Layered Double Perovskites (LDPs) is much greater than has hitherto been recognized, especially with the recent emergence of hybrid LDPs in which protonated amines play the role of some, or all, of the A cations.
2. In the case of inorganic LDPs, there is now an enormous family of compounds that are doubled due to ordering of different ions on the A, B, or X sites. Furthermore, these show an extensive range of functionalities, including remarkable magnetic, electronic, spectroscopic, electrochemical and catalytic properties.
3. The field of hybrid LDPs is less mature, but they show great promise, especially in the halide LDPs, where the low dimensionality facilitates the formation of important compounds, such as iodides, that do not normally form as 3D double perovskites.

FUTURE DIRECTIONS

1. Certain areas of the inorganic LDPs have been neglected to date, but would be worthy of future exploration. The absence of chalcogenide LDPs is particularly striking and could present some exciting opportunities for the future.
2. In the case of the hybrid LDPs, the focus hitherto has been largely on the halides of the post-transition metals, largely due to their relationship to the important hybrid perovskites of lead. We see many opportunities in the study of hybrid LDPs based on transition metals and rare-earths, where the magnetic and spectroscopic properties could be of great interest.
3. Beyond the current focus on hybrid LDP halides, there is also great scope for work in the area of LDPs containing polyatomic anionic linkers, in much the same way that this area has become very important for the 3D perovskites. Such linkers would include formates, hypophosphites, azides and cyanides, most of which are known to form 2D and 3D perovskites, some of them doubled.

DISCLOSURE STATEMENT

The authors are not aware of any affiliations, memberships, funding, or financial holdings that might be perceived as affecting the objectivity of this review.

ACKNOWLEDGMENTS

H.A.E. thanks the National Research Council (USA) for financial support through the Research Associate Program. L.M. and R.S. have been supported by the Department of Energy, Office of Science, Basic Energy Sciences, under Grant No. SC0012541. AKC acknowledges the Ras al Khaimah Centre for Advanced Materials for supporting this research.

LITERATURE CITED

1. Goldschmidt VM. 1926. Die gesetze der krystallochemie. *Naturwiss.* 14:477–485
2. Megaw HD. 1946. Crystal structure of double oxides of the perovskite type. *Proc. Phys. Soc.* 58:133
3. von Hippel A. 1950. Ferroelectricity, domain structure, and phase transitions of barium titanate. *Rev. Mod. Phys.* 22:221–237
4. Sleight AW, Gillson JL, Bierstedt PE. 1993. High-temperature superconductivity in the $BaPb_{1-x}Bi_xO_3$ system. *Solid State Commun.* 88:841–842
5. Wu MK, Ashburn JR, Torng CJ, Hor PH, Meng RL, et al. 1987. Superconductivity at 93 K in a new mixed-phase Y-Ba-Cu-O compound system at ambient pressure. *Phys. Rev. Lett.* 58:908–910
6. von Helmolt R, Wecker J, Holzapfel B, Schultz L, Samwer K. 1993. Giant negative magnetoresistance in perovskitelike $La_{2/3}Ba_{1/3}MnO_x$ ferromagnetic films. *Phys. Rev. Lett.* 71:2331–2333
7. Jin S, Tiefel TH, McCormack M, Fastnacht R, Ramesh R, Chen L. 1994. Thousandfold change in resistivity in magnetoresistive La-Ca-Mn-O films. *Science* 264:413–415
8. Li W, Wang Z, Deschler F, Gao S, Friend RH, Cheetham AK. 2017. Chemically diverse and multifunctional hybrid organic–inorganic perovskites. *Nat. Rev. Mater.* 2:16099
9. Kojima A, Teshima K, Shirai Y, Miyasaka T. 2009. Organometal halide perovskites as visible-light sensitizers for photovoltaic cells. *J. Am. Chem. Soc.* 131:6050–6051
10. Wang Xy, Gan L, Zhang Sw, Gao S. 2004. Perovskite-like metal formates with weak ferromagnetism and as precursors to amorphous materials. *Inorg. Chem.* 43:4615–4625
11. King G, Woodward PM. 2010. Cation ordering in perovskites. *J. Mater. Chem.* 20:5785–5796
12. Sarma D, Sampathkumaran E, Ray S, Nagarajan R, Majumdar S, et al. 2000. Magnetoresistance in ordered and disordered double perovskite oxide, Sr_2FeMoO_6. *Solid State Commun.* 114:465–468
13. Wei F, Deng Z, Sun S, Xie F, Kieslich G, et al. 2016. The synthesis, structure and electronic properties of a lead-free hybrid inorganic–organic double perovskite $(MA)_2KBiCl_6$ (MA = methylammonium). *Mater. Horiz.* 3:328–332
14. Sekiya T, Yamamoto T, Torii Y. 1984. Cation ordering in $(NaLa)(MgW)O_6$ with the perovskite structure. *B. Chem. Soc. Jpn.* 57:1859–1862
15. Yang M, Oró-Solé J, Rodgers JA, Jorge AB, Fuertes A, Attfield JP. 2011. Anion order in perovskite oxynitrides. *Nat. Chem.* 3:47–52
16. Wu Y, Halat DM, Wei F, Binford T, Seymour ID, et al. 2018. Mixed X-Site formate-hypophosphite hybrid perovskites. *Chem. Eur. J.* 24:11309–11313
17. Balz D, Plieth K. 1955. Die struktur des kaliumnickelfluorids, K_2NiF. *Z. Elektrochem.* 59:545–551
18. Bednorz JG, Müller KA. 1986. Possible high T_c superconductivity in the Ba-La-Cu-O system. *Z. Phys. B* 64:189–193
19. Ruddlesden S, Popper P. 1958. The compound $Sr_3Ti_2O_7$ and its structure. *Acta Crystallogr.* 11:54–55
20. Dion M, Ganne M, Tournoux M. 1981. Nouvelles familles de phases $M^{I}M^{II}_2Nb_3O_{10}$ a feuillets "perovskites". *Mater. Res. Bull.* 16:1429–1435
21. Jacobson A, Johnson JW, Lewandowski J. 1985. Interlayer chemistry between thick transition-metal oxide layers: synthesis and intercalation reactions of $K[Ca_2Na_{n-3}Nb_nO_{3n+1}]$ ($3 \leq n \leq 7$). *Inorg. Chem.* 24:3727–3729
22. Smith MD, Crace EJ, Jaffe A, Karunadasa HI. 2018. The diversity of layered halide perovskites. *Annu. Rev. Mater. Res.* 48:111–136
23. Vargas B, Ramos E, Pérez-Gutiérrez E, Alonso JC, Solis-Ibarra D. 2017. A direct bandgap copper–antimony halide perovskite. *J. Am. Chem. Soc.* 139:9116–9119
24. Battle PD, Green MA, Laskey NS, Millburn JE, Rosseinsky MJ, et al. 1996. Coupled metal-insulator and magnetic transitions in $LnSr_2Mn_2O_7$ (Ln = La, Tb). *Chem. Commun.* 207:767–

768
25. Seshadri R, Martin C, Maignan A, Hervieu M, Raveau B, Rao CNR. 1996. Structure and magnetotransport properties of the layered manganites $RE_{1.2}Sr_{1.8}Mn_2O_7$ (RE = La, Pr, Nd). *J. Mater. Chem.* 6:1585–1590
26. Clarke SJ, Hardstone KA, Michie CW, Rosseinsky MJ. 2002. High-temperature synthesis and structures of perovskite and $n = 1$ Ruddlesden-Popper tantalum oxynitrides. *Chem. Mater.* 14:2664–2669
27. Connor BA, Leppert L, Smith MD, Neaton JB, Karunadasa HI. 2018. Layered halide double perovskites: Dimensional reduction of $Cs_2AgBiBr_6$. *J. Am. Chem. Soc.* 140:5235–5240
28. Akamatsu H, Fujita K, Kuge T, Sen Gupta A, Togo A, et al. 2014. Inversion Symmetry Breaking by Oxygen Octahedral Rotations in the Ruddlesden-Popper $NaRTiO_4$ Family. *Phys. Rev. Lett.* 112:187602
29. Kanade K, Baeg J, Kong K, Kale B, Lee S, et al. 2008. A new layer perovskites $Pb_2Ga_2Nb_2O_{10}$ and $RbPb_2Nb_2O_7$: An efficient visible light driven photocatalysts to hydrogen generation. *Int. J. Hydrog. Energy* 33:6904–6912
30. Fjellvåg ØS, Armstrong J, Vajeeston P, Sjåstad AO. 2018. New insights into hydride bonding, dynamics, and migration in La_2LiHO_3 oxyhydride. *J. Phys. Chem. Lett.* 9:353–358
31. Park GE, Byeon SH. 1996. Correlation between Structures and Ionic Conductivities of $Na_2Ln_2Ti_3O_{10}$ (Ln = La, Nd, Sm, and Gd). *B Korean Chem. Soc* 17:168–172
32. Schaak RE, Mallouk TE. 2000. Prying apart Ruddlesden-Popper phases: Exfoliation into sheets and nanotubes for assembly of perovskite thin films. *Chem. Mater.* 12:3427–3434
33. Ma R, Sasaki T. 2015. Two-dimensional oxide and hydroxide nanosheets: Controllable high-quality exfoliation, molecular assembly, and exploration of functionality. *Acc. Chem. Res.* 48:136–143
34. ten Elshof JE, Yuan H, Gonzalez Rodriguez P. 2016. Two-dimensional metal oxide and metal hydroxide nanosheets: Synthesis, controlled assembly and applications in energy conversion and storage. *Adv. Energy Mater.* 6:1600355
35. Gönen ZS, Paluchowski D, Zavalij P, Eichhorn BW, Gopalakrishnan J. 2006. Reversible cation/anion extraction from $K_2La_2Ti_3O_{10}$: Formation of new layered titanates, $KLa_2Ti_3O_{9.5}$ and $La_2Ti_3O_9$. *Inorg. Chem.* 45:8736–8742
36. Toda K, Teranishi T, Ye ZG, Sato M, Hinatsu Y. 1999. Structural chemistry of new ion-exchangeable tantalates with layered perovskite structure: New dion–jacobson phase $Mca_2ta_3o_{10}$ (M = alkali metal) and ruddlesden–popper phase $na_2ca_2ta_3o_{10}$. *Mater. Res. Bull.* 34:971–982
37. Hyeon KA, Byeon SH. 1999. Synthesis and structure of new layered oxides, $M^{II}La_2Ti_3O_{10}$ (M = Co, Cu, and Zn). *Chem. Mater.* 11:352–357
38. Fukuoka H, Isami T, Yamanaka S. 2000. Crystal structure of a layered perovskite niobate kca_2nb_3o10. *J. Solid State Chem.* 151:40–45
39. Thangadurai V, Schmid-Beurmann P, Weppner W. 2001. Synthesis, structure, and electrical conductivity of A'$[A_2B_3O_{10}]$ (A' = Rb, Cs; A = Sr, Ba; B = Nb, Ta): New members of Dion-Jacobson-type layered perovskites. *J. Solid State Chem.* 158:279–289
40. Anderson MT, Greenwood KB, Taylor GA, Poeppelmeier KR. 1993. B-cation arrangements in double perovskites. *Prog. Solid State Chem.* 22:197–233
41. Toda K, Teranishi T, Takahashi M, Ye ZG, Sato M. 1998. Structural chemistry of new ion-exchangeable tantalates with layered perovskite structure: New reduced Ruddlesden-Popper phase, $Na_2Ca_2Ta_3O_{10}$. *Solid State Ion.* 113-115:501–508
42. Shannon RDT, Prewitt CT. 1969. Effective ionic radii in oxides and fluorides. *Acta Crystallogr. B* 25:925–946
43. Uma S, Gopalakrishnan J. 1993. $K_{1-x}La_xCa_{2-x}Nb_3O_{10}$, a layered perovskite series with variable interlayer cation density, and $LaCaNb_3O_{10}$, a novel layered perovskite oxide with no interlayer cations. *J. Solid State Chem.* 102:332–339

44. Nishimoto S, Matsuda M, Harjo S, Hoshikawa A, Kamiyama T, et al. 2006. Structure determination of $n = 1$ Ruddlesden–Popper compound $HLaTiO_4$ by powder neutron diffraction. *J. Eur. Ceram. Soc.* 26:725–729
45. Chen D, Jiao X, Xu R. 1999. Hydrothermal synthesis and characterization of the layered titanates $MLaTiO_4$ (M = Li, Na, K) powders. *Mater. Res. Bull.* 34:685–691
46. Toda K, Kurita S, Sato M. 1996. New layered perovskite compounds, $LiLaTiO_4$ and $LiEuTiO_4$. *J. Ceram. Soc. Jpn.* 104:140–142
47. Zhu BC, Tang KB. 2011. Rietveld refinement of $KLaTiO_4$ from X-ray powder data. *Acta Crystallogr. E* 67:i26–i26
48. Toda K, Kurita S, Sato M. 1995. Synthesis and ionic conductivity of novel layered perovskite compounds, $AgLaTiO_4$ and $AgEuTiO_4$. *Solid State Ion.* 81:267–271
49. Byeon SH, Park K, Itoh M. 1996. Structure and ionic conductivity of $NaLnTiO_4$; Comparison with those of $Na_2Ln_2Ti_3O_{10}$ (Ln = La, Nd, Sm, and Gd). *J. Solid State Chem.* 121:430–436
50. Toda K, Kameo Y, Kurita S, Sato M. 1996. Crystal structure determination and ionic conductivity of layered perovskite compounds $NaLnTiO_4$ (Ln = rare earth). *J. Alloys Compd.* 234:19–25
51. Reddy VR, Hwang DW, Lee JS. 2003. Effect of Zr substitution for Ti in $KLaTiO_4$ for photocatalytic water splitting. *Catal. Lett.* 90:39–43
52. Gupta AS, Akamatsu H, Strayer ME, Lei S, Kuge T, et al. 2016. Improper inversion symmetry breaking and piezoelectricity through oxygen octahedral rotations in layered perovskite family, LiR TiO_4 (R = Rare Earths). *Adv. Electron. Mater.* 2:1500196
53. Sen Gupta A, Akamatsu H, Brown FG, Nguyen MAT, Strayer ME, et al. 2017. Competing structural instabilities in the ruddlesden–popper derivatives $HRTiO_4$ (R = Rare Earths): Oxygen octahedral rotations inducing noncentrosymmetricity and layer sliding retaining Centrosymmetricity. *Chem. Mater.* 29:656–665
54. Akamatsu H, Fujita K, Kuge T, Gupta AS, Rondinelli JM, et al. 2019. A-site cation size effect on oxygen octahedral rotations in acentric Ruddlesden-Popper alkali rare-earth titanates. *Phys. Rev. Mater.* 5:065001
55. Su Y, Tsujimoto Y, Fujii K, Tatsuta M, Oka K, et al. 2018. Synthesis, crystal structure, and optical properties of lLayered perovskite scandium oxychlorides: Sr_2ScO_3Cl, $Sr_3Sc_2O_5Cl_2$, and $Ba_3Sc_2O_5Cl_2$. *Inorg. Chem.* 57:5615–5623
56. Kamegashira N, Meng J, Fujita K, Satoh H, Shishido T, Nakajima K. 2006. Study on the phase behavior of $BaEu_2Mn_2O_7$ through heat treatment of a single crystal. *J. Alloys Compd.* 408-412:603–607
57. Armstrong AR, Anderson PA. 1994. Synthesis and structure of a new layered niobium blue bronze: $Rb_2LaNb_2O_7$. *Inorg. Chem.* 33:4366–4369
58. Strayer ME, Gupta AS, Akamatsu H, Lei S, Benedek NA, et al. 2016. Emergent noncentrosymmetry and piezoelectricity driven by oxygen octahedral rotations in $n = 2$ Dion-Jacobson phase layer perovskites. *Adv. Funct. Mater.* 26:1930–1937
59. Kumada N, Kinomura N, Sleight AW. 1996. $CsLaNb_2O_7$. *Acta Crystallogr. C* 52:1063–1065
60. Toda K, Sato M. 1996. Synthesis and structure determination of new layered perovskite compounds, $ALaTa_2O_7$ and $ACa_2Ta_3O_{10}$(A = Rb, Li). *J. Mater. Chem.* 6:1067
61. Subramanian M, Gopalakrishnan J, Sleight A. 1988. New layered perovskites: $ABiNb_2O_7$ and $APb_2Nb_3O_{10}$ (A = Rb or Cs). *Mater. Res. Bull.* 23:837–842
62. Goff RJ, Keeble D, Thomas PA, Ritter C, Morrison FD, Lightfoot P. 2009. Leakage and proton conductivity in the predicted ferroelectric $CsBiNb_2O_7$. *Chem. Mater.* 21:1296–1302
63. Snedden A, Knight KS, Lightfoot P. 2003. Structural distortions in the layered perovskites $CsANb_2O_7$ (A = Nd, Bi). *J. Solid State Chem.* 173:309–313
64. Benedek NA. 2014. Origin of ferroelectricity in a family of polar oxides: The Dion-Jacobson phases. *Inorg. Chem.* 53:3769–3777
65. Mulder AT, Benedek NA, Rondinelli JM, Fennie CJ. 2013. Turning ABO_3 antiferroelectrics

into ferroelectrics: Design rules for practical rotation-driven ferroelectricity in double perovskites and $A_3B_2O_7$ Ruddlesden-Popper compounds. *Adv. Funct. Mater.* 23:4810–4820
66. Zhang R, Abbett BM, Read G, Lang F, Lancaster T, et al. 2016. $La_2SrCr_2O_7$: Controlling the tilting distortions of n = 2 Ruddlesden–Popper phases through A-Site cation order. *Inorg. Chem.* 55:8951–8960
67. Zhu T, Cohen T, Gibbs AS, Zhang W, Halasyamani PS, et al. 2017. Theory and neutrons combine to reveal a family of layered perovskites without inversion symmetry. *Chem. Mater.* 29:9489–9497
68. Zhu T, Khalsa G, Havas DM, Gibbs AS, Zhang W, et al. 2018. Cation exchange as a mechanism to engineer polarity in layered perovskites. *Chem. Mater.* 30:8915–8924
69. Autieri C, Barone P, Sławińska J, Picozzi S. 2019. Persistent spin helix in Rashba-Dresselhaus ferroelectric $CsBiNb_2O_7$. *Phys. Rev. Mater.* 3:084416
70. Honma T, Toda K, Ye ZG, Sato M. 1998. Concentration quenching of the Eu^{3+}-activated luminescence in some layered perovskites with two-dimensional arrangement. *J. Phys. Chem. Solids* 59:1187–1193
71. Argyriou DN, Bordallo HN, Campbell BJ, Cheetham AK, Cox DE, et al. 2000. Charge ordering and phase competition in the layered perovskite $LaSr_2Mn_2O_7$. *Phys. Rev. B* 61:15269–15276
72. Zhou G, Jiang X, Zhao J, Molokeev M, Lin Z, et al. 2018. Two-dimensional-layered perovskite $ALaTa_2O_7$:Bi^{3+} (A = K and Na) phosphors with versatile structures and tunable photoluminescence. *ACS Appl. Mater. Interfaces* 10:24648–24655
73. Liang Z, Tang K, Shao Q, Li G, Zeng S, Zheng H. 2008. Synthesis, crystal structure, and photocatalytic activity of a new two-layer Ruddlesden–Popper phase, $Li_2CaTa_2O_7$. *J. Solid State Chem.* 181:964–970
74. Galven C, Mounier D, Bouchevreau B, Suard E, Bulou A, et al. 2016. Phase transitions in the Ruddlesden–Popper Phase $Li_2CaTa_2O_7$: X-ray and neutron powder thermodiffraction, TEM, Raman, and SHG experiments. *Inorg. Chem.* 55:2309–2323
75. Zhang W, Fujii K, Niwa E, Hagihala M, Kamiyama T, Yashima M. 2020. Oxide-ion conduction in the Dion-Jacobson phase $CsBi_2Ti_2NbO_{10-\delta}$. *Nat. Commun.* 11:1224
76. Kim HG, Tran TT, Choi W, You TS, Halasyamani PS, Ok KM. 2016. Two new noncentrosymmetric n = 3 layered Dion-Jacobson perovskites: Polar $RbBi_2Ti_2NbO_{10}$ and nonpolar $CsBi_2Ti_2TaO_{10}$. *Chem. Mater.* 28:2424–2432
77. Acosta M, Novak N, Rojas V, Patel S, Vaish R, et al. 2017. $BaTiO_3$-based piezoelectrics: Fundamentals, current status, and perspectives. *Appl. Phys. Rev.* 4:041305
78. Zahedi E, Hojamberdiev M, Bekheet MF. 2015. Electronic, optical and photocatalytic properties of three-layer perovskite Dion-Jacobson phase $CsBa_2M_3O_{10}$ (M = Ta, Nb): A DFT study. *RSC Adv.* 5:88725–88735
79. Gopalakrishnan J, Sivakumar T, Thangadurai V, Subbanna GN. 1999. $A[Bi_3Ti_4O_{13}]$ and $A[Bi_3PbTi_5O_{16}]$ (A = K, Cs): New $n = 4$ and $n = 5$ members of the layered perovskite series, $A[A'_{n-1}B_nO_{3n+1}]$, and their hydrates. *Inorg. Chem.* 38:2802–2806
80. Zong X, Sun C, Chen Z, Mukherji A, Wu H, et al. 2011. Nitrogen doping in ion-exchangeable layered tantalate towards visible-light induced water oxidation. *Chem. Commun.* 47:6293
81. Maeda K, Eguchi M, Oshima T. 2014. Perovskite oxide nanosheets with tunable band-edge potentials and high photocatalytic hydrogen-evolution activity. *Angew. Chem. Int. Ed.* 53:13164–13168
82. Sato M, Toda K, Watanabe J, Uematsu K. 1993. Structure determination and silver ion conductivity of layered perovskite compounds $M_2La_2Ti_3O_{10}$ (M = K and Ag). *Nippon Kagaku Kaishi* :640–646
83. Rodionov IA, Silyukov OI, Utkina TD, Chislov MV, Sokolova YP, Zvereva IA. 2012. Photocatalytic properties and hydration of perovskite-type layered titanates $A_2Ln_2Ti_3O_{10}$ (A = Li, Na, K; Ln = La, Nd). *Russ. J. Gen. Chem.* 82:1191–1196
84. Gustin L, Hosaka Y, Tassel C, Aharen T, Shimakawa Y, et al. 2016. From tetrahedral to

octahedral iron coordination: layer compression in topochemically prepared $FeLa_2Ti_3O_{10}$. *Inorg. chem.* 55:11529–11537

85. Pratt JA, Shepherd AM, Hayward MA. 2015. Diamagnetic Ru^{2+} in $Na_2La_2Ti_2RuO_{10-x}$ ($0 < x < 2$): A series of complex oxides prepared by topochemical reduction. *Inorg. Chem.* 54:10993–10997
86. Schaak RE, Guidry EN, Mallouk TE. 2001. Converting a layer perovskite into a non-defective higher-order homologue: topochemical synthesis of $Eu_2CaTi_2O_7$. *Chem. Commun.* :853–854
87. Thangadurai V, Gopalakrishnan J, Subbanna GN. 1998. $Ln_2Ti_2O_7$ (Ln = La, Nd, Sm, Gd): a novel series of defective Ruddlesden-Popper phases formed by topotactic dehydration of $HLnTiO4^{+\dagger}$. *Chem. Commun.* 7:1299–1300
88. Abou-Warda S, Pietzuch W, Berghöfer G, Kesper U, Massa W, Reinen D. 1998. Ordered K_2NiF_4 structure of the solids $La_2Li_{1/2}M_{1/2}O_4$ (M(III) = Co, Ni, Cu) and the bonding properties of the MO6 polyhedra in various compounds of this type. *J. Solid State Chem.* 138:18–31
89. Abbattista F, Vallino M, Mazza D. 1985. Preparation and crystallographic characteristics of the new phase $La_2Au_{0.5}Li_{0.5}O_4$. *J. Less Common Met.* 110:391–396
90. Lehner AJ, Fabini DH, Evans HA, Hébert CA, Smock SR, et al. 2015. Crystal and electronic structures of complex bismuth iodides $A_3Bi_2I_9$ (A = K, Rb, Cs) related to perovskite: aiding the rational design of photovoltaics. *Chem. Mater.* 27:7137–7148
91. Teneze N, Mercurio D, Trolliard G, Frit B. 2000. Cation-deficient perovskite-related compounds $(Ba,La)_nTi_{n-1}O_{3n}$ (n = 4, 5, and 6): a Rietveld refinement from neutron powder diffraction data. *Mater. Res. Bull.* 35:1603–1614
92. Kemmler-Sack S, Wischert W, Treiber U. 1978. Uber hexagonale perowskite mit kationenfehlstellen. III Strukturbestimmungen an verbindungen vom Typ $Ba_2B_{1/3}{}^{III}{}_{2/3}Re^{VII}O_6$. *Z. Anorg. Allg. Chem.* 444:190–194
93. Yu R, Fan A, Li T, Yuan M, Wang J. 2017. Structure and luminescence properties of Eu^{3+}-doped trigonal double-perovskite $Ba_2Lu_{0.667}WO_6$. *Mater. Chem. Phys.* 196:75–81
94. Longo JM, Katz L, Ward R. 1965. Rhenium-containing complex metal oxides of the formula type $A^{II}{}_4Re^{VII}{}_2M^{II}O_{12}$. *Inorg. Chem.* 4:235–241
95. Herrmann M, Kemmler-Sack S. 1980. Über hexagonale perowskite mit kationenfehlstellen. XXII. Die polymorphie bei rhomboedrischen 12 L-Stapelvarianten im system $Sr_{4-x}Ba_xNiRe_2O_{12}$. *Z. Anorg. Allg. Chem.* 469:51–60
96. Rawl R, Lee M, Choi ES, Li G, Chen KW, et al. 2017. Magnetic properties of the triangular lattice magnets $A_4B'B_2O_{12}$ (A = Ba, Sr, La; B' = Co, Ni, Mn; B = W, Re. *Phys. Rev. B.* 95:174438
97. Rother H, Kemmler-Sack S. 1980. Uber hexagonale perowskite mit kationenfehlstellen. XIX. Die rhomboedrischen 12 L-Stapelvarianten vom Typ $Ba_3LaB^{III}(W_2VIO_{12})$. *Z. Anorg. Allg. Chem.* 465:179–182
98. Falk F, Hackbarth L, Lochbrunner S, Marciniak H, Küppers T, Köckerling M. 2018. RareearthmMetal tetracyanidoborate hydrate salts: structural, spectral, and thermal properties as well as the luminescence of dehydrated salts. *Z. Anorg. Allg. Chem.* 644:1495–1502
99. Saito M, Watanabe M, Kurita N, Matsuo A, Kindo K, et al. 2019. Successive phase transitions and magnetization plateau in the spin-1 triangular-lattice antiferromagnet $Ba_2La_2NiTe_2O_{12}$ with small easy-axis anisotropy. *Phys. Rev. B.* 100:064417
100. Doi Y, Wakeshima M, Tezuka K, Shan YJ, Ohoyama K, et al. 2017. Crystal structures, magnetic properties, and DFT calculation of B-site defected 12L-perovskites $Ba_2La_2MW_2O_{12}$ (M = Mn, Co, Ni, Zn). *J. Condens. Matter Phys.* 29:365802
101. Li Z, Sun J, Wang Y, You L, Lin JH. 2005. Structural and magnetic properties of $Ba_3La_3Mn_2W_3O_{18}$. *J. Solid State Chem.* 178:114–119
102. Kim SW, Zhang R, Halasyamani PS, Hayward MA. 2015. $K_4Fe_3F_{12}$: An Fe^{2+}/Fe^{3+} charge-ordered, ferrimagnetic fluoride with a cation-deficient, layered perovskite structure. *Inorg.*

Chem. 54:6647–6652
103. Liu S, Xu Y, Qu N, Zhang Y, Wang J, et al. 2017. Charge Ordering in $K_4Fe_3F_{12}$ from a first principles study. *ChemistrySelect* 2:714–719
104. Frenzen G, Kummer S, Massa W, Babel D. 1987. Tetragonale fluorperowskite $AM_{0,75}X?_{0,25}F_3$ mit Kationendefizit: $K_4Mn^{II}Mn_2{}^{III}F_{12}$ und $Ba_2Cs_2Cu_3F_{12}$. *Z. Anorg. Allg. Chem.* 553:75–84
105. Manaka H, Miyashita Y, Watanabe Y, Masuda T. 2007. Synthesis of double-layer perovskite fluoride $K_3Cu_2F_7$ with spin gap and orbital order. *J. Phys. Soc. Jpn.* 76:044710
106. Herdtweck E, Babel D. 1981. Röntgenographische einkristallstrukturbestimmungen an den kalium-kupfer(II)-fluoriden K_2CuF_4 und $K_3Cu_2F_7$. *Z. Anorg. Allg. Chem.* 474:113–122
107. Herdtweck E, Kummer S, Babel D. 1991. Cation-deficient perovskites $Ba_2A^IM_2{}^{II}F_9$ (M^{II} = Fe, Co, Ni, Zn) and their hexagonal layer structure. *Eur. J. Solid State Inorg. Chem.* 28:959–969
108. Vargas B, Torres-Cadena R, Rodríguez-Hernández J, Gembicky M, Xie H, et al. 2018. Optical, electronic, and magnetic engineering of <111> layered halide perovskites. *Chem. Mater.* 30:5315–5321
109. Tang G, Xiao Z, Hosono H, Kamiya T, Fang D, Hong J. 2018. Layered halide double perovskites $Cs_{3+n}M(II)_nSb_2X_{9+3n}$ (M = Sn, Ge) for photovoltaic applications. *J. Phys. Chem. Lett.* 9:43–48
110. Xu J, Liu JB, Wang J, Liu BX, Huang B. 2018. Prediction of novel p-type transparent conductors in layered double perovskites: A first-principles study. *Adv. Funct. Mater.* 28:1800332
111. Liu Z, Zhao X, Zunger A, Zhang L. 2019. Design of mixed-cation tri-layered Pb-Free halide perovskites for optoelectronic applications. *Adv. Electron. Mater.* 5:1900234
112. Li J, Yu Q, He Y, Stoumpos CC, Niu G, et al. 2018. $Cs_2PbI_2Cl_2$, all-Iinorganic two-dimensional Ruddlesden-Popper mixed halide perovskite with optoelectronic response. *J. Am. Chem. Soc.* 140:11085–11090
113. Li J, Stoumpos CC, Trimarchi GG, Chung I, Mao L, et al. 2018. Air-stable direct bandgap perovskite semiconductors: All-inorganic tin-based heteroleptic halides $A_xSnCl_yI_z$ (A = Cs, Rb). *Chem. Mater.* 30:4847–4856
114. Xu Z, Chen M, Liu SF. 2019. Layer-dependent ultrahigh-mobility transport properties in all-inorganic two-dimensional $Cs_2PbI_2Cl_2$ and $Cs_2SnI_2Cl_2$ perovskites. *J. Phys. Chem. C* 123:27978–27985
115. McCall KM, Stoumpos CC, Kontsevoi OY, Alexander GCB, Wessels BW, Kanatzidis MG. 2019. From 0D $Cs_3Bi_2I_9$ to 2D $Cs_3Bi_2I_6Cl_3$: dimensional expansion induces a direct band gap but enhances electron–phonon coupling. *Chem. Mater.* 31:2644–2650
116. Morgan EE, Mao L, Teicher SML, Wu G, Seshadri R. 2020. Tunable perovskite-derived bismuth halides: $Cs_3Bi_2(Cl_{1-x}I_x)_9$. *Inorg. Chem.* 59:3387–3393
117. Hodgkins TL, Savory CN, Bass KK, Seckman BL, Scanlon DO, et al. 2019. Anionic order and band gap engineering in vacancy ordered triple perovskites. *Chem. Commun.* 55:3164–3167
118. Kobayashi Y, Tsujimoto Y, Kageyama H. 2018. Property engineering in perovskites via modification of anion chemistry. *Annu. Rev. Mater. Res.* 48:303–326
119. Harada JK, Charles N, Poeppelmeier KR, Rondinelli JM. 2019. Heteroanionic materials by design: Progress toward targeted properties. *Adv. Mater.* 31:1805295
120. Fuertes A. 2006. Prediction of anion distributions using Pauling's second rule. *Inorg. Chem.* 45:9640–9642
121. Loureiro SM, Felser C, Huang Q, Cava RJ. 2000. Refinement of the crystal structures of strontium cobalt oxychlorides by neutron powder diffraction. *Chem. Mater.* 12:3181–3185
122. Tsujimoto Y, Yamaura K, Uchikoshi T. 2013. Extended Ni(III) oxyhalide perovskite derivatives: Sr_2NiO_3X (X = F, Cl). *Inorg. Chem.* 52:10211–10216
123. Knee CS, Weller MT. 2002. New layered manganese oxide halides. *Chem. Commun.* 2:256–257
124. Romero FD, Hayward MA. 2012. Structure and magnetism of the topotactically reduced oxychloride $Sr_4Mn_3O_{6.5}Cl_2$. *Inorg. Chem.* 51:5325–5331
125. Su Y, Tsujimoto Y, Fujii K, Tatsuta M, Oka K, et al. 2018. Synthesis, crystal structure, and

optical properties of layered perovskite scandium oxychlorides: Sr_2ScO_3Cl, $Sr_3Sc_2O_5Cl_2$, and $Ba_3Sc_2O_5Cl_2$. *Inorg. Chem.* 57:5615–5623
126. Yoo CY, Kim J, Kim SC, Kim SJ. 2018. Crystal structures of new layered perovskite-type oxyfluorides, $CsANb_2O_6F$ (A = Sr and Ca) and comparison with pyrochlore-type $CsNb_2O_5F$. *J. Solid State Chem.* 267:146–152
127. Tsujimoto Y, Yamaura K, Takayama-Muromachi E. 2012. Oxyfluoride chemistry of layered perovskite compounds. *Appl. Sci.* 2:206–219
128. Harada JK, Poeppelmeier KR, Rondinelli JM. 2019. Predicting the structure stability of layered heteroanionic materials exhibiting anion order. *Inorg. Chem.* 58:13229–13240
129. Wang Y, Tang K, Zhu B, Wang D, Hao Q, Wang Y. 2015. Synthesis and structure of a new layered oxyfluoride Sr_2ScO_3F with photocatalytic property. *Mater. Res. Bull.* 65:42–46
130. Choy JH, Kim JY, Kim SJ, Sohn JS, Han OH. 2001. New Dion-Jacobson-type layered perovskite oxyfluorides, $ASrNb_2O_6F$ (A = Li, Na, and Rb). *Chem. Mater.* 13:906–912
131. Su Y, Tsujimoto Y, Matsushita Y, Yuan Y, He J, Yamaura K. 2016. High-pressure synthesis, crystal structure, and magnetic properties of Sr_2MnO_3F: A new member of layered perovskite oxyfluorides. *Inorg. Chem.* 55:2627–2633
132. Kobayashi Y, Tian M, Eguchi M, Mallouk TE. 2009. Ion-exchangeable, electronically conducting layered perovskite oxyfluorides. *J. Am. Chem. Soc.* 131:9849–9855
133. Needs RL, Weller MT. 1995. Synthesis and structure of Ba_2InO_3F: oxide/fluoride ordering in a new K_2NiF_4 superstructure. *J. Chem. Soc., Chem. Commun.* 7:353
134. Tarasova NA, Animitsa IE. 2018. The influence of the nature of halogen on the local structure and intercalation of water in oxyhalides Ba_2InO_3X (X = F, Cl, Br). *Opt. Spectrosc.* 124:163–166
135. Needs RL, Weller MT, Scheler U, Harris RK. 1996. Synthesis and structure of Ba_2InO_3X (X = F, Cl, Br) and Ba_2ScO_3F; oxide/halide ordering in K_2NiF_4-type structures. *J. Mater. Chem.* 6:1219
136. Galasso F, Darby W. 1963. Preparation and Properties of Sr_2FeO_3F. *J. Phys. Chem.* 67:1451–1453
137. Case GS, Hector AL, Levason W, Needs RL, Thomas MF, Weller MT. 1999. Syntheses, powder neutron diffraction structures and Mössbauer studies of some complex iron oxyfluorides: $Sr_3Fe_2O_6F_{0.87}$, Sr_2FeO_3F and $Ba_2InFeO_5F_{0.68}$. *J. Mater. Chem.* 9:2821–2827
138. Hector AL, Hutchings JA, Needs RL, Thomas MF, Weller MT. 2001. Structural and Mössbauer study of Sr_2FeO_3X (X = F, Cl, Br) and the magnetic structure of Sr_2FeO_3F. *J. Mater. Chem.* 11:527–532
139. Yoo CY, Hong KP, Kim SJ. 2007. A new layered perovskite, $KSrNb_2O_6F$, by powder neutron diffraction. *Acta Crystallogr. C* 63:i63–i65
140. Subramanian M, Aravamudan G, Subba Rao G. 1983. Oxide pyrochlores — A review. *Prog. Solid State Ch.* 15:55–143
141. Yoo CY, Kim SJ. 2008. Dimensional modification of oxyfluoride lattice: Preparation and structure of A'ANb_2O_6F (A' = Na, K, A = Ca, Sr). *J. Phys. Chem. Solids* 69:1475–1478
142. Hector AL, Knee CS, MacDonald AI, Price DJ, Weller MT. 2005. An unusual magnetic structure in Sr_2FeO_3F and magnetic structures of K_2NiF_4-type iron(iii) oxides and oxide halides, including the cobalt substituted series $Sr_2Fe_{1-x}Co_xO_3Cl$. *J. Mater. Chem.* 15:3093
143. Knee CS, Zhukov AA, Weller MT. 2002. Crystal structures and magnetic properties of the manganese oxide chlorides Sr_2MnO_3Cl and $Sr_4Mn_3O_{8-y}Cl_2$. *Chem. Mater.* 14:4249–4255
144. Ronning F, Kim C, Feng DL, Marshall DS, Loeser AG, et al. 1998. Photoemission evidence for a remnant fermi surface and a d-wave-like dispersion in insulating $Ca_2CuO_2Cl_2$. *Science* 282:2067–2072
145. Kohsaka Y, Azuma M, Yamada I, Sasagawa T, Hanaguri T, et al. 2002. Growth of Na-Doped $Ca_2CuO_2Cl_2$ single crystals under high pressures of several GPa. *J. Am. Chem. Soc.* 124:12275–12278

146. Muller-Buschbaum H, Boje J. 1991. Zur kenntnis eines halogenooxo-cobaltats(III): $Sr_8Co_6O_{15}Cl_4$. *Z. Anorg. Allg. Chem.* 592:73–78
147. Vaknin D, Miller LL, Zarestky JL. 1997. Stacking of the square-lattice antiferromagnetic planes in $Ca_2CuO_2Cl_2$. *Phys. Rev. B* 56:8351–8359
148. Knee CS, Weller MT. 2002. Synthesis and structure of cobalt(II) oxide halides — $Sr_2CoO_2X_2$ (X = Cl, Br). *J. Solid State Chem.* 168:1–4
149. Knee CS, Weller MT. 2003. Synthesis and structure of new layered copper oxide iodides, $Sr_2CuO_2I_2$ and $Sr_2Cu_3O_4I_2$. *J. Mater. Chem.* 13:1507
150. Lafond A, Leynaud O, André G, Bourée F, Meerschaut A. 2002. Magnetic properties of $Ln_2Ti_2S_2O_5$ compounds and magnetic structure of $Tb_2Ti_2S_2O_5$. *J. Alloys Compd.* 338:185–193
151. Yashima M, Ogisu K, Domen K. 2008. Structure and electron density of oxysulfide $Sm_2Ti_2S_2O_{4.9}$, a visible-light-responsive photocatalyst. *Acta Crystallogr. B* 64:291–298
152. Goga M, Seshadri R, Ksenofontov V, Gütlich P, Tremel W. 1999. $Ln_2Ti_2S_2O_5$ (Ln = Nd, Pr, Sm): a novel series of defective Ruddlesden–Popper phases. *Chem. Commun.* 2006:979–980
153. Rutt OJ, Hill TL, Gál ZA, Hayward MA, Clarke SJ. 2003. The cation-deficient Ruddlesden-Popper oxysulfide $Y_2Ti_2O_5S_2$ as a layered sulfide: Topotactic potassium intercalation to form $KY_2Ti_2O_5S_2$. *Inorg. Chem.* 42:7906–7911
154. Wang Q, Nakabayashi M, Hisatomi T, Sun S, Akiyama S, et al. 2019. Oxysulfide photocatalyst for visible-light-driven overall water splitting. *Nat. Mater.* 18:827–832
155. Fuertes A. 2015. Metal oxynitrides as emerging materials with photocatalytic and electronic properties. *Mater. Horiz.* 2:453–461
156. Wu Y, Lazic P, Hautier G, Persson K, Ceder G. 2013. First principles high throughput screening of oxynitrides for water-splitting photocatalysts. *Energy Environ. Sci.* 6:157–168
157. Fuertes A. 2012. Chemistry and applications of oxynitride perovskites. *J. Mater. Chem.* 22:3293
158. Oshima T, Ichibha T, Qin KS, Muraoka K, Vequizo JJM, et al. 2018. Undoped layered perovskite oxynitride $Li_2LaTa_2O_6N$ for photocatalytic CO_2 reduction with visible light. *Angew. Chem.* 130:8286–8290
159. Diot N, Marchand R, Haines J, Léger J, Macaudière P, Hull S. 1999. Crystal structure determination of the oxynitride Sr_2TaO_3N. *J. Solid State Chem.* 146:390–393
160. Tobías G, Oró-Solé J, Beltrán-Porter D, Fuertes A. 2001. New family of Ruddlesden-Popper strontium niobium oxynitrides: $(SrO)(SrNbO_{2-x}N)_n (n = 1, 2)$. *Inorg. Chem.* 40:6867–6869
161. Bouri M, Aschauer U. 2018. Bulk and surface properties of the Ruddlesden–Popper oxynitride Sr_2TaO_3N. *Phys. Chem. Chem. Phys.* 20:2771–2776
162. Wei S, Xu X. 2018. Boosting photocatalytic water oxidation reactions over strontium tantalum oxynitride by structural laminations. *Appl. Catal. B* 228:10–18
163. Tobías G, Beltrán-Porter D, Lebedev OI, Van Tendeloo G, Rodríguez-Carvajal J, Fuertes A. 2004. Anion ordering and defect structure in Ruddlesden-Popper strontium niobium oxynitrides. *Inorg. Chem.* 43:8010–8017
164. Kim YI, Woodward PM, Baba-Kishi KZ, Tai CW. 2004. Characterization of the structural, optical, and dielectric properties of oxynitride perovskites AMO_2N (A = Ba, Sr, Ca; M = Ta, Nb). *Chem. Mater.* 16:1267–1276
165. 2019. Ammonothermal synthesis of the mixed-valence nitrogen-rich europium tantalum Ruddlesden-Popper phase $Eu^{II}Eu^{III}{}_2Ta_2N_4O_3$. *Eur. J. Inorg. Chem.* 2019:2304–2311
166. Marchand R. 1982. Structure cristalline De Nd_2AlO_3N. Détermination de L'Ordre oxygène-azote par diffraction de neutrons
167. Pelloquin D, Hadermann J, Giot M, Caignaert V, Michel C, et al. 2004. Novel, oxygen-deficient n = 3 RP-Member $Sr_3NdFe_3O_{9-\delta}$ and its topotactic derivatives. *Chem. Mater.* 16:1715–1724
168. Raveau B, Hervieu M, Pelloquin D, Michel C, Retoux R. 2005. A large family of iron Ruddlesden-Popper relatives: From oxides to oxycarbonates and oxyhydroxides. *Z. Anorg.*

Allg. Chem 631:1831–1839
169. Jantsky L, Okamoto H, Demont A, Fjellvåg H. 2012. Tuning of water and hydroxide content of intercalated Ruddlesden-Popper-type oxides in the $PrSr_3Co_{1.5}Fe_{1.5}O_{10-\delta}$ system. *Inorg. Chem.* 51:9181–9191
170. Pelloquin D, Barrier N, Flahaut D, Caignaert V, Maignan A. 2005. Two new hydrated oxyhydroxides $Sr_3Co_{1.7}Ti_{0.3}O_5(OH)_2xH_2O$ and $Sr_4Co_{1.6}Ti_{1.4}O_8(OH)_2xH_2O$ derived from the RP n = 2 and 3 members: Structural and magnetic behavior versus temperature. *Chem. Mater.* 17:773–780
171. Motohashi T, Raveau B, Caignaert V, Pralong V, Hervieu M, et al. 2005. Spin glass to weak ferromagnetic transformation in a new layered cobaltite: Consequence of topotactic reactions with water at room temperature. *Chem. Mater.* 17:6256–6262
172. Bang J, Matsuishi S, Hiraka H, Fujisaki F, Otomo T, et al. 2014. Hydrogen ordering and new polymorph of layered perovskite oxyhydrides: $Sr_2VO_{4-x}H_x$. *J. Am. Chem. Soc.* 136:7221–7224
173. Hayward MA. 2002. The hydride anion in an extended transition metal oxide array: $LaSrCoO_3H_{0.7}$. *Science* 295:1882–1884
174. Hernandez OJ, Geneste G, Yajima T, Kobayashi Y, Okura M, et al. 2018. Site selectivity of hydride in early-transition-metal Ruddlesden–Popper oxyhydrides. *Inorg. Chem.* 57:11058–11067
175. Schwarz H. 1991. *Neuartige hydrid-oxide der seltenen erden: Ln_2LiHO_3 mit Ln.* na
176. Kobayashi G, Hinuma Y, Matsuoka S, Watanabe A, Iqbal M, et al. 2016. Pure H-conduction in oxyhydrides. *Science* 351:1314–1317
177. Minervini L, Grimes RW, Kilner JA, Sickafus KE. 2000. Oxygen migration in $La_2NiO_{4+\delta}$. *J. Mater. Chem.* 10:2349–2354
178. Numata Y, Sanehira Y, Ishikawa R, Shirai H, Miyasaka T. 2018. Thiocyanate containing two-dimensional cesium lead iodide perovskite, $Cs_2PbI_2(SCN)_2$: Characterization, photovoltaic application, and degradation mechanism. *ACS Appl. Mater. Interfaces* 10:42363–42371
179. Chiang YH, Li MH, Cheng HM, Shen PS, Chen P. 2017. Mixed cation thiocyanate-based pseudohalide perovskite solar cells with high efficiency and stability. *ACS Appl. Mater. Interfaces* 9:2403–2409
180. Labram J, Venkatesan N, Takacs C, Evans H, Perry E, et al. 2017. Charge transport in a two-dimensional hybrid metal halide thiocyanate compound. *J. Mater. Chem. C* 5
181. Headspith DA, Sullivan E, Greaves C, Francesconi MG. 2009. Synthesis and characterisation of the quaternary nitride-fluoride $Ce_2MnN_3F_{2-\delta}$. *Dalton Trans.* :9273
182. Nazarenko O, Kotyrba MR, Wörle M, Cuervo-Reyes E, Yakunin S, Kovalenko MV. 2017. Luminescent and photoconductive layered lead halide perovskite compounds comprising mixtures of cesium and guanidinium cations. *Inorg. Chem.* 56:11552–11564
183. Soe CMM, Stoumpos CC, Kepenekian M, Traoré B, Tsai H, et al. 2017. Newtype of 2D perovskites with alternating cations in the interlayer space, $(C(NH_2)_3)(CH_3NH_3)_nPb_nI_{3n+1}$: Structure, properties, and photovoltaic performance. *J. Am. Chem. Soc.* 139:16297–16309
184. McNulty JA, Lightfoot P. 2020. Unprecedented tin iodide perovskite-like structures featuring ordering of organic moieties. *Chem. Commun.* 56:4543–4546
185. Guo YY, McNulty JA, Mica NA, Samuel IDW, Slawin AMZ, et al. 2019. Structure-directing effects in (110)-layered hybrid perovskites containing two distinct organic moieties. *Chem. Commun.* 55:9935–9938
186. Salah MBH, Mercier N, Allain M, Zouari N, Giovanella U, Botta C. 2019. Mechanochromic and electroluminescence properties of a layered hybrid perovskite belonging to the <110> series. *Eur. J. Inorg. Chem.* :4527–4531
187. Guo YY, Yang LJ, Biberger S, McNulty JA, Li T, et al. 2020. Structural diversity in layered hybrid perovskites, A_2PbBr_4 or AA'$PbBr_4$, templated by small disc-shaped amines. *Inorg. Chem.* 59:12858–12866

188. Nazarenko O, Kotyrba MR, Yakunin S, Aebli M, Rainò G, et al. 2018. Guanidinium-formamidinium lead iodide: A layered perovskite-related compound with red luminescence at room temperature. *J. Am. Chem. Soc.* 140:3850–3853
189. Daub M, Hillebrecht H. 2018. First representatives of (210)-oriented perovskite variants – Synthesis, crystal structures and properties of the new 2D hybrid perovskites $A[HC(NH_2)_2]PbI_4$; A = $[C(NH_2)_3]$, $[HSC(NH_2)_2]$. *Z. Kristallogr. Cryst. Mater.* 233:555–564
190. Mao L, Stoumpos CC, Kanatzidis MG. 2019. Two-dimensional hybrid halide perovskites: Principles and promises. *J. Am. Chem. Soc.* 141:1171–1190
191. Mercier N. 2019. Hybrid halide perovskites: Discussions on terminology and materials 58:17912–17917
192. Smith MD, Connor BA, Karunadasa HI. 2019. Tuning the luminescence of layered halide perovskites. *Chem. Rev.* 119:3104–3139
193. Kieslich G, Sun S, Cheetham AK. 2015. An extended tolerance factor approach for organic–inorganic perovskites. *Chem. Sci.* 6:3430–3433
194. Fu Y, Hautzinger MP, Luo Z, Wang F, Pan D, et al. 2019. Incorporating large A cations into lead iodide perovskite cages: relaxed Goldschmidt tolerance factor and impact on exciton–phonon interaction. *ACS Cent. Sci.* 5:1377–1386
195. Hautzinger MP, Pan D, Pigg AK, Fu Y, Morrow DJ, et al. 2020. Band edge tuning of two-dimensional Ruddlesden-Popper perovskites by *A* cation size revealed through nanoplates. *ACS Energy Lett.* 5:1430–1437
196. Fu Y, Jiang X, Li X, Traore B, Spanopoulos I, et al. 2020. Cation engineering in two-dimensional Ruddlesden-Popper lead iodide perovskites with mixed large *A*-site cations in the cages. *J. Am. Chem. Soc.* 142:4008–4021
197. Liang M, Lin W, Lan Z, Meng J, Zhao Q, et al. 2020. Electronic structure and trap states of two-dimensional Ruddlesden-Popper perovskites with the relaxed Goldschmidt tolerance factor. *ACS Appl. Electron. Mater.* 2:1402–1412
198. Li X, Fu Y, Pedesseau L, Guo P, Cuthriell S, et al. 2020. Negative pressure engineering with large cage cations in 2D halide perovskites causes lattice softening. *J. Am. Chem. Soc.* 142:11486–11496
199. Jana MK, Janke SM, Dirkes DJ, Dovletgeldi S, Liu C, et al. 2019. Direct-bandgap 2D silver–bismuth iodide double perovskite: The structure-directing influence of an oligothiophene spacer cation. *J. Am. Chem. Soc.* 141:7955–7964
200. Bi LY, Hu YQ, Li MQ, Hu TL, Zhang HL, et al. 2019. Two-dimensional lead-free iodide-based hybrid double perovskites: crystal growth, thin-film preparation and photocurrent responses. *J. Mater. Chem. A* 7:19662–19667
201. Bi LY, Hu TL, Li MQ, Ling BK, Lassoued MS, et al. 2020. Template effects in Cu(I)–Bi(III) iodide double perovskites: a study of crystal structure, film orientation, band gap and photocurrent response. *J. Mater. Chem. A* 8:7288–7296
202. Mao L, Teicher SML, Stoumpos CC, Kennard RM, DeCrescent RA, et al. 2019. Chemical and structural diversity of hybrid layered double perovskite halides. *J. Am. Chem. Soc.* 141:19099–19109
203. McClure ET, McCormick AP, Woodward PM. 2020. Four lead-free layered double perovskites with the $n = 1$ Ruddlesden-Popper structure. *Inorg. Chem.* 59:6010–6017
204. Guo W, Liu X, Han S, Liu Y, Xu Z, et al. 2020. Room-temperature ferroelectric material composed of a two-dimensional metal halide double perovskite for X-ray detection. *Angew. Chem. Int. Ed.* 59:13879–13884
205. Connor BA, Biega RI, Leppert L, Karunadasa HI. 2020. Dimensional reduction of the small-bandgap double perovskite $Cs_2AgTlBr_6$. *Chem. Sci.* 11:7708–7715
206. Xu Z, Liu X, Li Y, Liu X, Yang T, et al. 2019. Exploring lead-free hybrid double perovskite crystals of $(BA)_2CsAgBiBr_7$ with large mobility-lifetime product toward X-ray detection. *Angew. Chem.* 131:15904–15908

207. Zhang W, Hong M, Luo J. 2020. Halide double perovskite ferroelectrics. *Angew. Chem. Int. Ed.* 59:9305–9308
208. Castro-Castro LM, Guloy AM. 2003. Organic-based layered perovskites of mixed-valent gold(I)/gold(III) iodides. *Angew. Chem. Int. Ed.* 42:2771–2774
209. Yao Y, Kou B, Peng Y, Wu Z, Li L, et al. 2020. $(C_3H_9NI)_4AgBiI_8$: a direct-bandgap layered double perovskite based on a short-chain spacer cation for light absorption. *Chem. Commun.* 56:3206–3209
210. Lassoued MS, Bi LY, Wu Z, Zhou G, Zheng YZ. 2020. Piperidine-induced Switching of the direct band gaps of Ag(I)/Bi(III) bimetallic iodide double perovskites. *J. Mater. Chem. C* 8:5349–5354
211. Sheng R, Ho-Baillie A, Huang S, Chen S, Wen X, et al. 2015. Methylammonium lead bromide perovskite-based solar cells by vapor-assisted deposition. *J. Phys. Chem. C* 119:3545–3549
212. Evans HA, Schueller EC, Smock SR, Wu G, Seshadri R, Wudl F. 2017. Perovskite-related hybrid noble metal iodides: Formamidinium platinum iodide $[(FA)_2Pt^{IV}I_6]$ and mixed-valence methylammonium gold iodide $[(MA)_2Au^{I}Au^{III}I_6]$. *Inorg. Chim. Acta* 468:280–284
213. Wei F, Deng Z, Sun S, Zhang F, Evans DM, et al. 2017. Synthesis and properties of a lead-free hybrid double perovskite: $(CH_3NH_3)_2AgBiBr_6$. *Chem. Mater.* 29:1089–1094
214. Tran TT, Panella JR, Chamorro JR, Morey JR, McQueen TM. 2017. Designing indirect–direct bandgap transitions in double perovskites. *Mater. Horiz.* 4:688–693
215. Yu Y, Shang R, Chen S, Wang BW, Wang ZM, Gao S. 2017. A series of bimetallic ammonium AlNa formates. *Chem. Eur. J.* 23:9857–9871
216. Chen S, Shang R, Wang BW, Wang ZM, Gao S. 2018. Electric and magnetic transitions with 90° turning of polarizations in a layered perovskite of $[NH_4Cl]_2[Ni(HCOO)_2(NH_3)_2]$. *APL Mater.* 6:114205
217. Shi C, Ye L, Gong ZX, Ma JJ, Wang QW, et al. 2020. Two-dimensional organic–inorganic hybrid rare-earth double perovskite ferroelectrics. *J. Am. Chem. Soc.* 142:545–551
218. Evans H, Wu Y, Seshadri R, Cheetham A. 2020. Perovskite-related ReO_3-type structures. *Nat. Rev. Mater.* 5:196–213
219. Kieslich G, Forse AC, Sun S, Butler KT, Kumagai S, et al. 2016. Role of amine–cavity interactions in determining the structure and mechanical properties of the ferroelectric hybrid perovskite $[NH_3NH_2]Zn(HCOO)_3$. *Chem. Mater.* 28:312–317
220. Wu Y, Shaker S, Brivio F, Murugavel R, Bristowe PD, Cheetham AK. 2017. $[Am]Mn(H_2POO)_3$: A new family of hybrid perovskites based on the hypophosphite ligand. *J. Am. Chem. Soc.* 139:16999–17002
221. Evans HA, Deng Z, Collings IE, Wu Y, Andrews JL, et al. 2019. Polymorphism in $M(H_2PO_2)_3$ (M = V, Al, Ga) compounds with the perovskite-related ReO_3 structure. *Chem. Commun.* 55:2964–2967